Nonlinear numerical analysis of non-planar rectangular hollow structural section connections

by

Nathan Knox

B.S., Florida Institute of Technology, 2017

A THESIS

submitted in partial fulfillment of the
requirements for the degree

MASTER OF SCIENCE

Department of Civil Engineering
Carl R. Ice College of Engineering

KANSAS STATE UNIVERSITY
Manhattan, Kansas

2022

Approved by:

Major Professor
Dr. Christopher Jones

Copyright

© Nathan Knox 2022.

Abstract

This thesis summarizes a study performed to evaluate the ability of General Purpose and Component Based Finite Element solvers to accurately predict the strength and deformation characteristics of non-planar Rectangular Hollow Structural Section joints (RHSS). There are no known empirical equations for non-planar connections. Therefore, these connections can only be designed by means of advanced analysis or by using empirical equations developed based on experimental tests of planar connections. The geometry of non-planar connections tends to result in the branch connecting at the corner of a chord, resulting in a stiffer connection. Therefore, it is reasonable to hypothesize that non-planar connections may have increased capacity compared to standard planar connections, at least when considering the chord wall plastification failure mode.

A Research Oriented Finite Element program (Abaqus) and Design Oriented Finite Element program (Idea StatiCa) were used in this study. A verification and validation procedure was used in this study to (1) verify the mathematical models were properly calibrated and had an acceptable level of error and (2) validate that the mathematical models adequately predict the physical behavior of the real connection. Experimental data used to validate the numerical models was gathered from a combination of previously published papers and original experiments performed at the Kansas State University Civil Engineering Laboratory.

The scope of the experimental program performed for this thesis was too limited to provide a definitive answer to the research question; however, the results are favorable and suggest that each finite element strategy can be used to accurately analyze and design complex RHSS joints. The planar numerical models created in Abaqus predicted the relevant System Response Quantities (SRQs), local deformation and plastic strain, within 5% when compared to available experimental data, IDEA StatiCa consistently under-predicted the capacity of these connections. When comparing Abaqus numerical results of bird beak connections to

AISC empirical equations for a planar analogue connection the bird beak connection was shown to have significantly more chord wall plastification capacity for the connections studied. Bird beak connections had $> 9\%$ more capacity than their planar analogue in all cases. More research in this area is needed to evaluate if non-planar connections have more capacity than planar connections when considering a more complete range of connection dimensions, branch angles, and loading types.

Table of Contents

List of Figures vii

List of Tables x

List of Nomenclature xi

Acknowledgements xii

1 Introduction 1

1.1 Current Analysis Standards 5

1.2 Welding Considerations 6

2 Finite Element Method 8

2.1 Background of the Finite Element Method 9

2.1.1 Finite Element Method used as a Tool for Design and Research of HSS Connections 10

2.2 Element Types 11

2.3 Finite Element Software 12

2.4 Component Based Finite Element Analysis 13

2.5 Quantities of Interest (Ultimate Load Criteria) 15

2.5.1 Chord Wall Plastification 16

2.5.2 Punching Shear 17

2.6 Nonlinear Solution Settings 18

3 Validation using Published Data 20

3.1 Published Experimental Studies . . . 20
3.1.1 Numerical Model Setup . . . 21
3.1.2 Material Properties . . . 22
3.1.3 Sensitivity Study . . . 27
3.1.4 Results . . . 41

4 Validation Using Experimental Data . . . 43
4.1 Bird Beak Connections . . . 43
4.2 Prototype Geometry . . . 44
4.2.1 Material Properties . . . 44
4.3 Numerical Models Setup . . . 45
4.3.1 IDEA StatiCa X-specimen . . . 45
4.3.2 Abaqus X-Specimen . . . 46
4.3.3 IDEA StatiCa T-specimens . . . 51
4.3.4 IDEA Member T-Specimen Model . . . 52
4.3.5 Abaqus T-Specimens . . . 52
4.4 Results and Discussion . . . 55
4.4.1 Measuring Local Deflection . . . 57
4.4.2 T-Specimen . . . 59
4.4.3 X-Specimen . . . 64

5 Conclusions and Recommendations . . . 75
5.1 Further Studies . . . 77

Bibliography . . . 79

A Fabrication Drawings . . . 87

List of Figures

1.1 Minneapolis Convention Center Roof Truss (Tamboli, 2010) 1

1.2 Launch Vehicle Access Space Truss 4

1.3 Uniplanar and Multiplanar RHS Joint Example 6

1.4 Code Guidance (North American Standards) 7

2.1 Available Element Types in Abaqus 13

2.2 Component Method Example Assessment and Assessment [8] 14

2.3 Super element IDEA StatiCa 16

2.4 Ultimate Failure Mode Criteria (CEN, 2021) 17

2.5 Example of Punching Shear Failure 18

3.1 Uniplanar RHS Connection (Bu and Packer, 2020) 21

3.2 Weld Representation in Abaqus Numerical Model 22

3.3 IDEA StatiCa Numerical Model 23

3.4 True Stress-Strain Conversion, Region ii 25

3.5 Power Regression of Hardening Region 26

3.6 True Stress Strain Match 26

3.7 Numerical Model Engineering Stress-Strain Data Fit 27

3.8 Sensitivity Analysis Process 28

3.9 Element Type Comparisons - Force Displacement Curves 30

3.10 Abaqus Mesh Refinement 34

3.11 X-0.5-21-25O Element Size Sensitivity Study 35

3.12 Abaqus Boundary Conditions 37

3.13 X-0.5-21-25O Boundary Condition Sensitivity Study 37

3.14 Direct Forming Process . . . 39
3.15 Continuous Forming Process . . . 39
3.16 X-0.5-21-25O Corner Material Property Sensitivity Study . . . 40
3.17 Model Results with Results of Sensitivity Study Incorporated . . . 41
3.18 Planar Connection Results . . . 42

4.1 T-Specimen Assembly and Fabrication . . . 45
4.2 Idea Statica X-Specimen Isometric . . . 47
4.3 Backer Sensitivity Study . . . 48
4.4 T-specimen Branch-Chord Mesh . . . 49
4.5 Thickened Branch to Represent Backer Sleeve in Abaqus . . . 50
4.6 X-Specimen Material Assignments . . . 51
4.7 IDEA Connection Internal Forces . . . 52
4.8 T-Specimen, Idea Member . . . 53
4.9 Abaqus Model Setup . . . 54
4.10 Abaqus Mesh . . . 55
4.11 T-Specimen Branch-Chord Mesh . . . 56
4.12 T-Specimen Material Assignments . . . 56
4.13 Local Deformation Reference Nodes . . . 58
4.14 Local Deformation of Cross Section . . . 59
4.15 T-Specimen Compression Results . . . 61
4.16 T-Specimen Tension Results . . . 63
4.17 X-Specimen Compression Results . . . 66
4.18 X-Specimen Tension Results . . . 68
4.19 Assumed Punching Shear Distribution . . . 72
4.20 Shear Distribution Bird Beak Connection . . . 73
4.21 Shear Distribution Planar Connection . . . 73
4.22 Shear Distribution Bird Beak Connection . . . 74

4.23 Shear Distribution Bird Beak Connection 74

List of Tables

3.1 Sensitivity Analysis for Specimen X-0.5-21-25O (Mesh Size) 29

3.2 GCI Results - Plastic Strain Convergence 33

3.3 Effects of Boundary Condition Study 36

Nomenclature

β	Branch to Chord Width Ratio $b1/b_o$
ϵ	Strain
ϵ_T	True Strain
γ	Half Wall Slenderness Ratio $b_0/2 * t_0$
σ	Stress
σ_T	True Stress
E	Youngs Modulus
F_y	Yield strength
GCI	Grid Convergence Index
U	Potential Energy

Acknowledgments

I would like to first thank my thesis advisor, Dr. Christopher Jones for providing guidance throughout the entire process of writing this thesis. It would not have been possible to finish this research without the expertise provided by Dr. Jones. Dr. Jones dedicated significant time to help educate me on material failure modes, model verification/validation, and all other information needed to complete this research. I would also like to thank the other members of my graduate committee, Drs. Melhem and Schiff, who provided valuable inputs to this project.

Additional help came from the engineers at IDEA StatiCa. Dr. Martin Vild provided theoretical background and practical guidance related to the IDEA StatiCa programs. Dave Eckrote, Juraj Sabatka, and Vojtech Chalupa also provided guidance related to the IDEA StatiCa programs.

Clifford Temple served one of the most important roles in this research program and lead the effort to fabricate the experimental specimens. Clifford used his expertise to cut, clean, and weld four steel specimens as well as several tensile coupons for the required material testing effort.

Finally, I would like to thank my wife Samantha Knox for her patience and constant support through the many long nights and weekends required to finish this thesis.

Chapter 1

Introduction

Hollow Structural Sections are essential to modern engineering. These shapes are strong, aesthetically appealing, and valuable in many applications. The hollow nature of tubes allows them to be efficient in bending, torsion, and compression. Engineers have long recognized these beneficial properties and have used hollow structural sections (HSS) for various structures, including offshore platforms, bridges, towers, amusement park rides, and other unique structures.

Figure 1.1: Minneapolis Convention Center Roof Truss (Tamboli, 2010)

These tubular structures, especially those built with rectangular tubes, are typically made with tubes oriented at right angles to allow for easy assembly and strength prediction. However, tubes joined at varying angles can produce structures of architectural brilliance and structural efficiency. Some examples of these structures can be seen in Figures 1.1 and 1.2. Figure 1.1 is a picture of a space truss in the roof of the Minneapolis Convention Center. Figure 1.2 shows another space truss, which is the structure for a launch vehicle access platform constructed by the United Launch Alliance in Cape Canaveral, Florida. Due to its particular use, this platform must rotate about a single fixed support and span around

the circumference of a Vulcan rocket. The designers of this platform determined that the most efficient structural framing would be a space truss built using a rectangular hollow structural section (RHS). The space truss had to be assembled to provide adequate global strength and stiffness while allowing access for personnel and rolling support equipment.

To meet these requirements, the final design resulted in joint configurations with multiple non-planar RHS connected to the same chord member, as seen in Figures 1.2a and 1.2b. As can be seen in this section, there are scenarios where the use of non-planar HSS connections is required or at least beneficial. However, after reviewing the primary North American and European building codes, there currently exists no prescribed way for analyzing these connections [4, 25, 20].

An inability to analyze a complex structure is a common issue in engineering. Structural engineers typically design structures and connections based on empirical equations derived from a limited number of numerical/experimental tests. To design general connections, such as the RHS space joints studied in this thesis, a more sophisticated tool is necessary [26]. Finite element analysis (FEA) can be used to analyze virtually any geometry/loading that can be fabricated and is used often in the Aerospace and Naval industries but is not often used in Civil Engineering. This is likely due to the lack of formal FEA education in universities and the lack of guidance in design codes [2, 26].

Progress has been made in recent years to facilitate the use of FEA in tubular connection design and Civil Engineering in general. Many comprehensive research papers have been published showing the critical considerations that must be made in FEA models and demonstrating these models' accuracy compared to experimental tests. Eurocodes are, at the time of this writing, publishing a new document EN1994-1-14 Design Assisted by Finite Element Analysis. This is the first and only Civil Engineering standard published on FEA methodology known to the author of this paper. One significant driver in the use of FEA to design civil structures is the software IDEA StatiCa. This program uses a novel method to analyze the force distribution in a connection using the power of finite element analysis and provides the strength of the connection components using traditional code equations. See Section 2.4 for explanation of the method.

Since there are no known code-based equations for non-planar connections, the only viable empirical equations that can be used to design these connections are those meant for planar connections. Due to the increase in material stiffness near the corner of RHS it is reasonable to hypothesize that non-planar connections would offer more capacity than their planar counterparts, at-least in plastification failure modes.The primary purpose of this paper is to (1) evaluate the use of General Purpose and Component Based Finite Element finite element solvers to predict the strength characteristics of Rectangular Hollow Structural Section connections in steel structures and (2) compare the strength of the non-planar connections considered to an analogous planar connection.

The author hopes that this information, along with other literature posted in the field, will help to expedite the adoption of finite element analysis as a tool used in the design of steel structures at a rate closer to the aerospace and naval industries. Benchmarks used in this case have been gathered from a mix of previously published and original experimental data. Numerical models have been created in Abaqus CAE and IDEA StatiCa and compared to this empirical data to determine (i) the feasibility of analyzing these connections with finite element analysis without being an expert in advanced methodologies and (ii) modeling parameters that produce reasonably accurate results without excess computational burden.

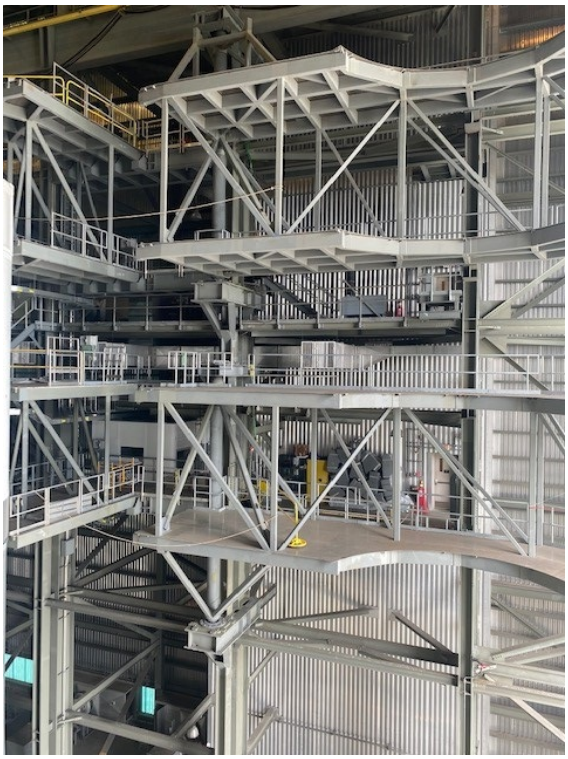

(a)

(b)

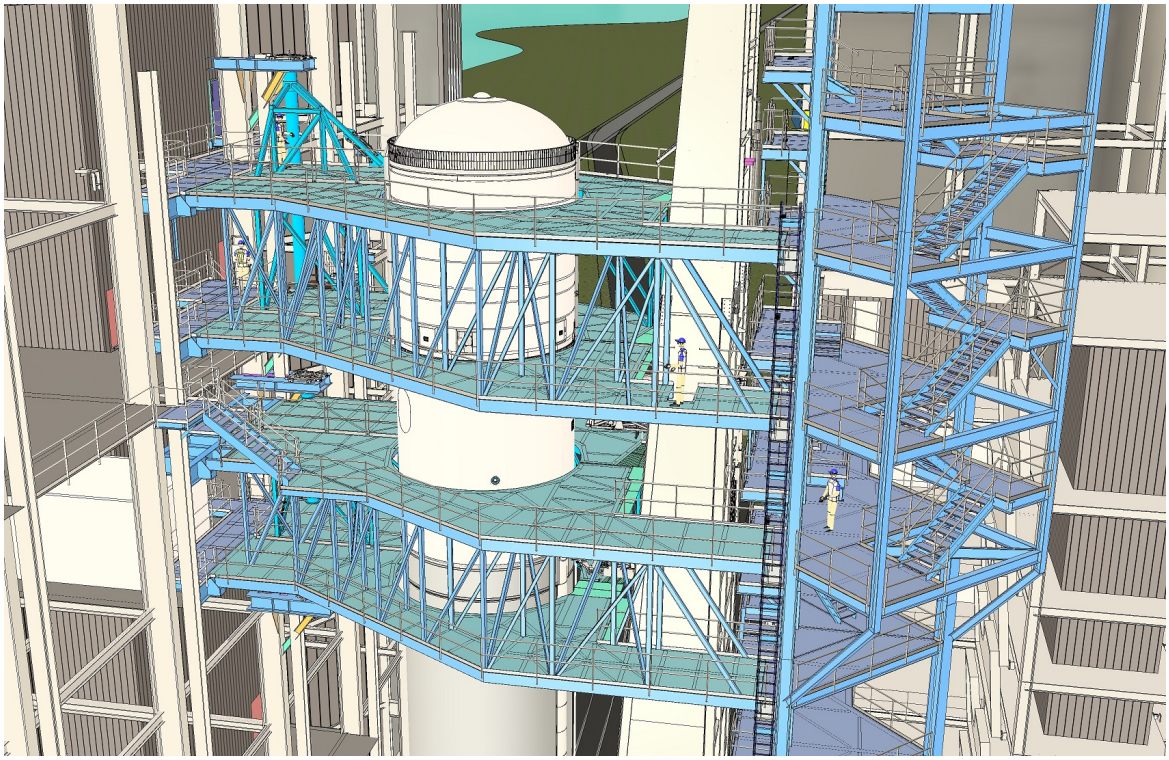

(c)

Figure 1.2: (a)Launch Vehicle Access Platforms Open (b) Launch Vehicle Access Platform Connection Detail (c) Launch Vehicle Access Platform Isometric

1.1 Current Analysis Standards

In North America, the primary governing code for the design and analysis of steel structures is the American Institute of Steel Constructions (AISC) Steel Construction Manual, 15^{th} edition [4]. The provisions in this manual are primarily based on research sponsored and synthesized by the Committee for International Development and Education on Construction of Tubular structures (CIDECT), which has been studying the behavior of tubular joints since the 1960s. The guidance in the AISC manual has also been thoroughly reviewed by the International Institute of Welding (IIW) subcommission XVE on Tubular structures. IIW does not produce its own code, but some of its recommendations have been incorporated in CIDECT design guides and AWS 2015. The most relevant CIDECT design guide to this research is CIDECT design guide #3 for Rectangular Hollow Section (RHS) Joints under Predominately Static Loading [49].

Requirements for HSS connections are given in the AISCM Chapter K. The manual clearly states in the opening paragraph that the design recommendations are for members that lie in the same plane only, like the joint seen in 1.3a and that design of joints that do not meet this criterion must be designed using an alternate code, or by rational analysis. CIDECT Design Guide #3 offers guidance for multi-planar connections and connections to the corner of a chord known as "bird beak" connections. The multiplanar joint recommendations are based on research by Liu and Wardenier ([40], [41], [42], [43]). The referenced research papers are not publicly available for review. However, the CIDECT design tables do state that the design strengths are limited to braces at 90-degree angles only, such as seen in Figure 1.3b.

Since strength limits are not provided in CIDECT Design Guide #3 the North American engineer is left with only the choice to design non-planar RHS connections by rational analysis. The commentary for AISCM Chapter K states the following in regard to designing HSS connections by rational analysis (also see Figure 1.4):

- All failure modes must be checked, including the modes not referenced in Ch. K (such as local buckling of the chord face)

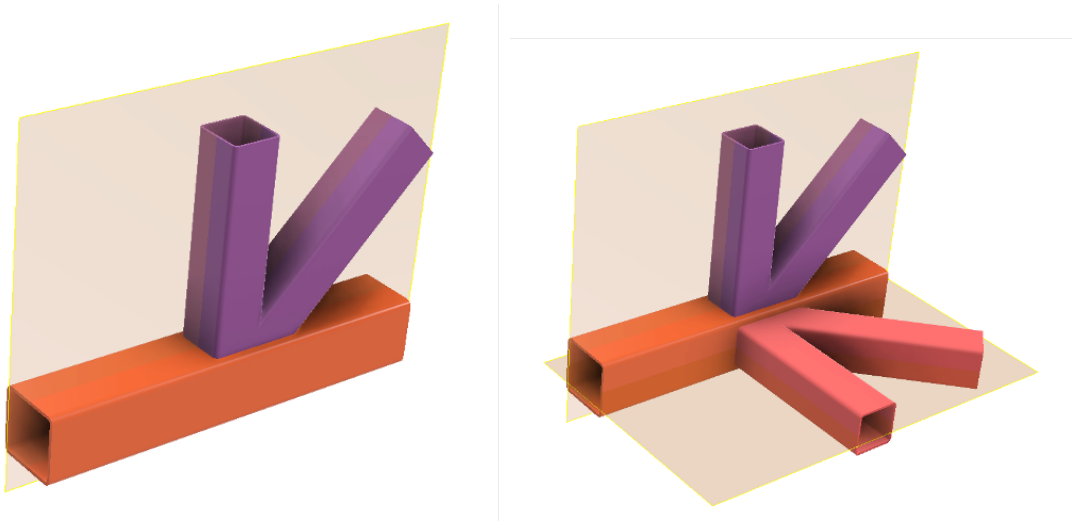

(a) (b)

Figure 1.3: (a) Uniplanar RHS Joint (b) Multiplanar RHS Joint

- When inelastic finite element analysis is used, peak strains in the thick shell (TxTxT) elements should not exceed 0.02/T at the nominal capacity, where T is the thickness in inches
- No deformation limit is explicitely given in the manual, but the 3% local deformation limit provided in CIDECT Design Guide #3 is recommended
- No guidance is provided concerning analysis types, element types, solvers, etc.

1.2 Welding Considerations

Typical orthogonal RHS connections are straightforward to weld. Plates connect at a right angle and can be fillet welded or groove welded using prequalified welding procedures. However, with non-planar connections, plates may connect at excessively acute or obtuse angles, making welding more of a challenge. Fillet welds can be used to connect these angled plates, but at excessive angles, the leg of the weld tends to get very large to reach the required weld throat thickness. Partial joint penetration (PJP) welds are an option for tubes at a large angle and can be used without backer material, but for thin-walled tubes, PJP welds are

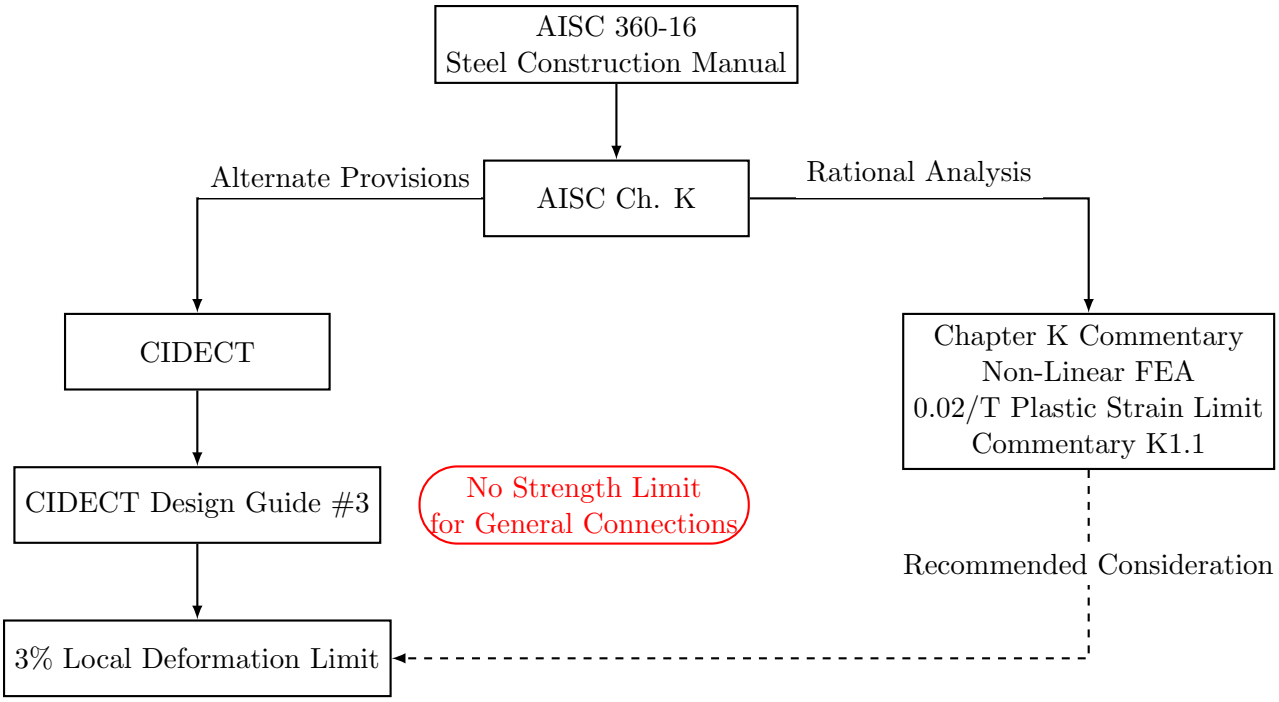

Figure 1.4: Code Guidance (North American Standards)

often very weak relative to the strength of the tube. For some tube thicknesses, PJP welds cannot be used, as can be seen in Section 4.2.

When the low relative strength of PJP welds is not adequate for a connection, or when the thickness of the tube does not permit a PJP weld, a complete joint penetration (CJP) weld must be used. CJP welds, when made with an appropriate weld filler metal, match the strength of the base metal. When CJP welds are made between RHS members, a backer must be provided behind the weld filler as shown in Figure 4.5, or a unique welding procedure must be qualified and tested, and a 6GR certified welder must fabricate the joint [20]. There is no prequalified welding procedure for this weld in the AISC specification or the Eurocodes. Because of these unique and often costly requirements, it is typically recommended not to specify CJP welds. However, in situations such as those considered in this paper CJP welds may be the best option.

Chapter 2

Finite Element Method

The non-planar joints of interest in this study have few limitations, allowing a wide range of joint topologies. This makes it challenging, if not impossible, to use first principles and experimental tests to develop empirical design equations, instead a more general solution method is needed. The Finite Element Method (FEM) is a powerful tool that has been used for decades to analyze complex structures in civil, mechanical, and aerospace engineering and is well suited to use in the design of structural joints with many possible joint configurations.

The FEM is a tool used to approximate the behavior of complex structures, by breaking the structure into many smaller, finite, pieces. These finite pieces, often called elements, are linked to each-other by a continuous field parameter, like displacement, or temperature, at discrete locations, often called nodes. The values between the nodes are determined by polynomial interpretation, based on the order of the element. To solve the value of the field parameter at the nodes a system of partial differential equations (PDEs) must be solved. There is often no closed-formed analytical solution for this system of equations, so numerical methods must be used to approximate the solution. These numerical methods, though inexact, can provide results that are accurate enough for use in the design of engineering structures. This Section will establish the validity of using finite element analysis in design by reviewing the historical use of the method and will establish some of the main theoretical considerations when setting up models.

2.1 Background of the Finite Element Method

In 1953 M.J. Turner and Ray Clough had the difficult task of assessing the stiffness of a Delta airplane wing. At first Turner and Clough applied a standard bar assemblage approach, which provided unsatisfactory accuracy. In an attempt to find a more accurate approach Mr. Turner suggested dividing the wing skin into triangular segments, analyzing the stiffness of the triangles with simplifying assumptions, and then combining the components to obtain the stiffness of the complete wing system. To solve the stiffness of the wing Turner and Clough created the FEM [18].

Turner and Clough would go on to publish a paper documenting their work a few years later and officially coin the term FEM [60]. Clough would be the one to carry on the development of the FEM in the academic world. Clough was a Civil Structural Engineering professor at Berkeley and made important impacts to the field. In 1962 the US Corps of engineers funded a practical finite element study to determine the stress in a cracked gravity dam [19]. In 1967 Clough applied the FEM to determine soil stresses in earthen embankment [17] and throughout the late 60's and early 70's added to the general industry knowledge studying the behavior of various element and loading types [13, 51, 16, 33, 12].

After the theoretical basis of FEM was widely validated many groups began developing software programs in the 60's and 70's to allow for easier access to the method. Clough and others at UC Berkeley developed SAP IV for earthquake engineering of Civil structures, NASA sponsored the development of NASTRAN to be used for analysis of Aerospace structures, and a Norwegian ship company, Det Norske, created a program called Sesam for structural analysis of ships and offshore structures. After the introduction of these programs, the FEM became widely used in almost every industry including Aerospace, Civil, Biomedical, and Naval.

As computer power grew at the end of the decade, so did the popularity of the FEM. In Civil engineering the FEM became specifically popular as a research tool. Experimental testing is, without a doubt, the most reliable and accurate method that can be used to measure the strength and serviceability of steel connections. However, the cost and difficulty

associated with experimental work typically limit the scope of research programs. The FEM offers a cheaper and relatively more manageable way to expand the range of programs to check a wider possibility of input parameters.

2.1.1 Finite Element Method used as a Tool for Design and Research of HSS Connections

The use of the FEM in civil engineering has been so prevalent in the past 40 years an attempt will not be made here to summarize the scope of the research in the field. Instead, the progression of FEM used specifically for HSS connection research will be examined. Puthli and RS [52] is the earliest published research that utilized finite element analysis to check the strength of HSS connections and at the time showed good agreement between numerical and experimental models. The use of the FEM in HSS connection research only grew in popularity in the 1990's [22, 61, 39] and is a standard of practice today, with essentially every connection research program using numerical analysis. [45, 63, 48, 59, 34, 10].

While the FEM has been used universally for steel connection research, adoption in industry has lagged behind academia. Historically, numerical methods have primarily been used in the design of civil structural joints in exceptional circumstances only, such as joints on accelerators at CERN [6] and assessment of aging infrastructure [28, 29, 47]. This is because the development of finite element models for connections can require a great deal of time and expertise. However, the popularity of finite element analysis for design purposes is proliferating. In North America, the governing steel design committee, AISC, permits non-linear finite element analysis to design and analyze steel connections in AISC 360-16 Appendix 1 but does not provide robust guidance for model parameters. In Europe, the design of steel connections by finite element analysis is not only permitted but specific finite element guidance will also be given in Eurocodes 3: Part 1-14 Design Assisted by Finite Element Analysis.

Several companies have also developed design programs that utilize the power of finite element analysis to design steel connections. These programs include Hilti Profis,

VOESTALPINE Profildesigner, and IDEA StatiCa. These programs use a method called the Component-Based FEM, which is explained in Section 2.4.

Likely, the most notable of these programs is IDEA StatiCa Connection, which has been used in this research and offers a means for a practicing engineer to utilize the power of FEA without advanced knowledge of a general-purpose program, such as Abaqus or ANSYS. IDEA StatiCa has been used on many large projects worldwide, such as the Helsinki Olympic stadium, the Thames Tideway Tunnel in London, the Museum of the future in Dubai, and the Jakarta International Velodrome.

The commercial FEA programs noted previously are often linked directly to 3-dimensional Building Information Models (BIM). For example, IDEA StatiCa can automatically create a finite element model from Tekla Structures or Revit design models [30]. As the power of the modern computer continues to grow and software improves, designers and engineers increasingly rely on BIM. As this trend continues, it is fair to assume that engineers will also increasingly rely on FEA models of connections to increase design efficiency.

2.2 Element Types

The main two classes of element types that can be used to model the body of HSS members are shell elements and solid elements. In general, shell elements are more computationally efficient due to their ability to accurately represent the bending stiffness of slender objects with few degrees of freedom. Solid elements require multiple elements through the thickness of a member, which significantly increases the number of nodes in a model and increases the computing power required. Due to this, most early research programs on HSS connections utilized shell elements with great success [21, 39, 61].

Shell elements are more computationally efficient than solid elements but aren't well suited for modeling of some features, such as welds and bolts [62]. As computing power grew in the 2000s, more connection research programs utilized solid elements due to their ability to accurately model connectors and contact [67, 14]. This trend has continued to the present day, with many of the most recent research programs opting to use solid elements

[45, 63, 59, 10, 34, 35].

There are several types of solid elements, the most popular of which are Tetrahedral (TET) and Hexahedral (HEXs) elements. As can be seen in Figure 2.2 TET elements are volumetric elements with triangles on each face. HEXs elements are volumetric elements with a rectangle on each face. Every element, solid and shell, can be of varying orders. For example, TET and HEXs elements are commonly available in linear and quadratic orders. Linear elements have nodes at the corners only and interpolate the displacement between the corner nodes with a linear function. Quadratic elements have mid-side nodes, as seen in Figure 2.2, and can interpolate the displacement between the nodes with a quadratic polynomial shape function. Due to this increased flexibility, quadratic elements are typically able to achieve higher accuracy with fewer elements [31].

Automatic meshers use TET elements because they can easily be used to create a mesh on any geometry; for this reason, TET elements have become more popular. Over the years design and manufacturing methods have improved, and so has the complexity of many designs. Traditionally, HEXs elements are thought to be more accurate elements but cannot easily be used to mesh complex geometry. Since the demand for automatic meshing has increased, many researchers have studied the performance of TET elements. These studies have found that quadratic TETs can match, and in some cases even beat, the performance of HEXs elements in mechanical stress simulations [15, 55]. TETs ability to outperform Hexes is largely due to TETs inherent ability to conform to complex geometry, thus reducing the geometric error of the mesh discretization.

2.3 Finite Element Software

This study utilized both a full featured finite element program, Abaqus by Dassault systems, and a Component Based Finite Element program called IDEA StatiCa. Abaqus is one of the most widely used programs for research and offers many types of analysis and element types. IDEA StatiCa is design software that offers relatively fewer input options and allows for accelerated and simplified analyses for the practicing engineer. Both model types have

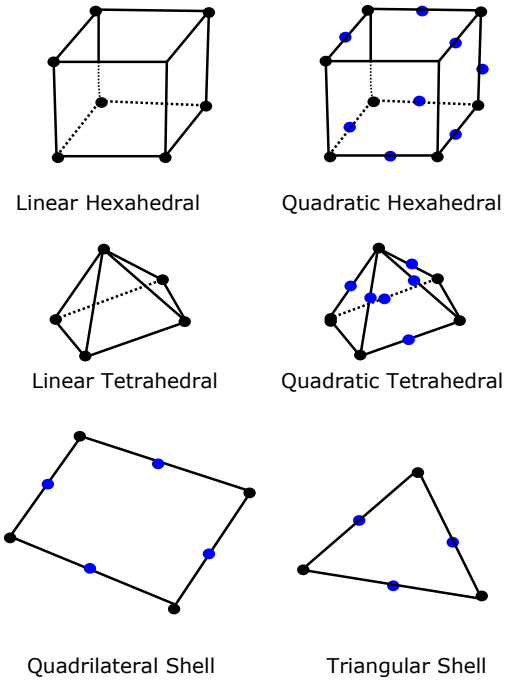

Figure 2.1: Available Element Types in Abaqus

been used here to investigate the predictive capability of each.

2.4 Component Based Finite Element Analysis

The Component Based FEM (CBFEM) is a combination of the component method and the FEM. This method was developed in a joint R&D project between the Czech Technical University and software company IDEA StatiCa to provide a way for engineers to design general connections, which don't fit a predefined template.

The traditional method of connection design is a curve fitting method. In this method empirical equations are created from a comprehensive set of experiments. These methods are, of course, limited to the types of connections previously studied and cannot be extended to a general connection set. A more general approach, the component method, has existed for some time that has aimed to facilitate analysis of a wider range of connections. This method involves assuming the initial internal force distribution in the connection, decomposing the connection into individual components, assigning a stiffness to each component based on force direction and previous testing, and reassembling the connection to determine global

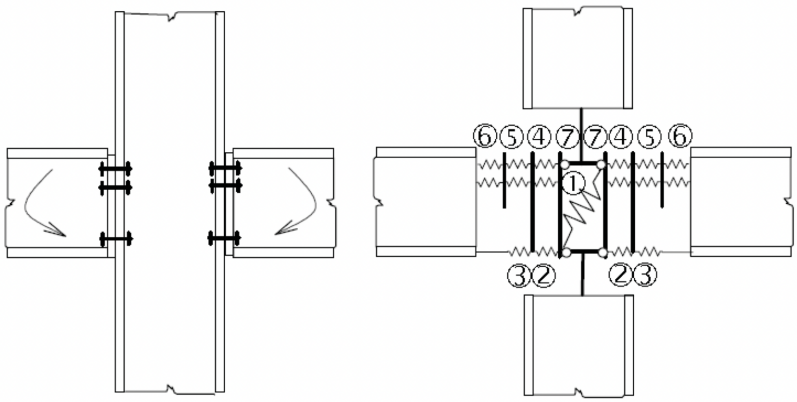

Figure 2.2: Component Method Example Assessment and Assessment [8]

joint moment-rotational behavior. An example of a joint analyzed with this method can be seen in Figure 2.2.

This method is more general than empirical equations and has even been investigated as a means to generalize the CIDECT design equations for tubular joints [66, 32]. However, this method is still limited by the amount of connections that can be tested to determine their internal force distribution [54] and typically requires the use of software, as its implementation by hand is quite complex. The CBFEM combines the power of the component method with the ability of the FEM to accurately determine the internal force distribution without testing for each joint configuration.

As discussed in Section 2.1 finite element analysis is well regarded as a research tool which, when properly calibrated, can produce highly accurate results. Research oriented finite element models (ROFEM's) are often extremely detailed, including explicitly modeled connectors such as bolts and welds and material properties obtained from physical tests. Including these details in design models would be both time and cost prohibitive; therefore, some simplifications need to be made.

In IDEA StatiCa Connection, the leading CBFEM software, bolts and welds are modeled with special 2d elements and multi-point constraints and plate materials are represented with a simplified bi-linear stress-strain diagram, with a nominal yield value. Bolts are modeled with non-linear springs that represent the bolt shank and a "fan" of interpolation elements that connect the shank to the plate edges. The force-deformation characteristics of the

bolt in tension and shear are derived analytically based on guidance from VDI 2230 and EN 1993-1-8:2006. These values have been shown to match well with experimental data [64]. Welds are modeled with Multi-Point Constraints (MPC's) and a special elastic-plastic weld element. MPC's connect plates at a weld joint without requiring nodes to be aligned between the plates. MPC's transfer displacement perfectly on either side of the constraint and therefore do not properly represent the stiffness of the weld. To account for this IDEA StatiCa places a special elasto-plastic weld element between the plates, allowing for plastic redistribution of forces between the MPC's [65].

The force in bolts and welds are determined by FEA as reported above, but the capacity of each is checked by the governing design code of the region. In North America design checks are governed by AISC Chapter J3 for bolts and welds are checked per AISC Chapter J2 [65]. Plates are checked against a limiting strain as reported in Section 2.5.

One difficulty when creating finite element models of connections is determining how to include the elastic stiffness of the member. Several approaches could be taken, but the one selected by IDEA StatiCa is to place a condensed super element between the center node of the connection and the ends of the members. This super element moves constraints away from the edge of the connection model and allows the edges of the shell model to deform. This super element is elastic only, all plastic deformation is maintained in the connection.

2.5 Quantities of Interest (Ultimate Load Criteria)

The AISC manual and CIDECT design guides reference several possible failure modes for welded HSS connections. Those failure modes are chord wall plastification, punching shear, chord wall buckling, branch wall buckling, and weld failure. To limit the scope of this research every possible failure mode was not considered in the analysis. Failure modes checked were chord wall plastification and punching shear. Buckling was not considered as it is assumed to occur less often than punching shear and plastification failures. As described in Sections 2.5.1 and 4.5 a limiting local deflection and plastic strain were used to represent plastification and punching shear limits. The AISC manual and CIDECT design guides do not provide

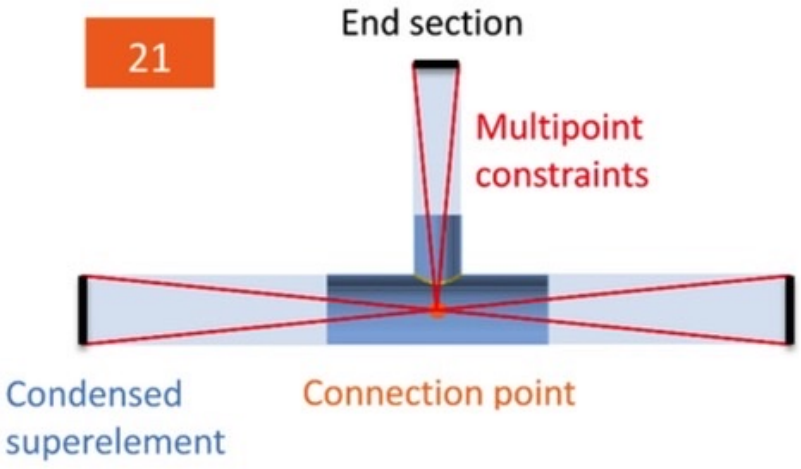

Figure 2.3: Super element IDEA StatiCa

comprehensive guidance for these quantities of interest when finite element models are used for design. However, Eurocodes Part 1-14: Design assisted by finite element analysis gives guidance for material non-linear analysis [25]. This document requires that the ultimate limit state for Material Non-linear Analysis (MNLA) be taken as the smaller value of C1 and C2 as shown in Figure 2.4. The ultimate load from criterion C1 is the maximum load on the load deformation curve, before excess plastification, or buckling. The ultimate load criterion C2 is based on a tolerable strain or deflection, as given by relevant building codes or research.

2.5.1 Chord Wall Plastification

One possible failure mode of HSS connections is chord wall plastification. Chord wall plastification occurs when a significant portion of the chord face around the intersection of brace and chord yields. This yielding may result in a distinct peak load, as shown in criterion C1 of Figure 2.4, or in the case of flexible connection, the resisting load may continue to increase well past a reasonable deflection limit. To control reasonable joint flexibility there have been studies performed to determine the most appropriate local deflection limits in welded HSS connections. Perhaps the most cited of these studies is the work done by Lu

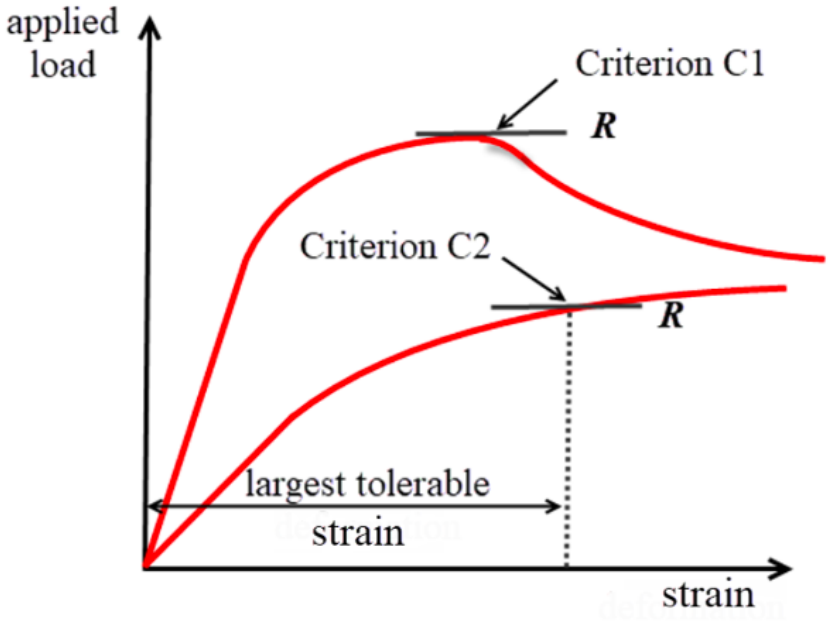

Figure 2.4: Ultimate Failure Mode Criteria (CEN, 2021)

in 1994 titled Deformation Limit for the Ultimate Strength of Hollow Section Joints [68]. In this work Lu and others determined a reasonable local deformation limit by plotting the local deformation of various HSS connections with distinct peak loads, with load deformation curves resembling criterion C1 in Figure 2.4. Lu found that local indentation of the chord face ranged from 2.5%-4% in these tests and thus determined that 3% chord face indentation is a reasonable flexibility limit for chord faces without a pronounced peak load.

Lu's work on this topic has been extremely influential and has been adopted by AISC, CIDECT, AWS and IIW [49, 50] and has been referenced in many research programs. This 3 percent limit has also been adopted for use as a primary code check in the design based finite element program used in this research, IDEA StatiCa Connection. This 3 percent limit will be used as a quantity of interest in all numerical and experimental models.

2.5.2 Punching Shear

Punching shear is another possible failure mode in welded HSS connections that has been considered in this research program. Punching shear occurs when the chord web member

ruptures before ultimate load is reached in a ductile failure state. This failure mode is common in stiff connections at areas of stress concentrations, particularly near the weld toe. An example of this failure can be seen in Figure 2.5. Material fracture is difficult to predict and must be calibrated for each connection geometry [10, 62, 9]. As an alternative it has been proposed to use a limiting plastic strain of 5% instead of attempting a more sophisticated fracture analysis [25, 64]. This plastic strain limit has also been adopted by IDEA StatiCa Connection and has been used as a limiting value in this research program.

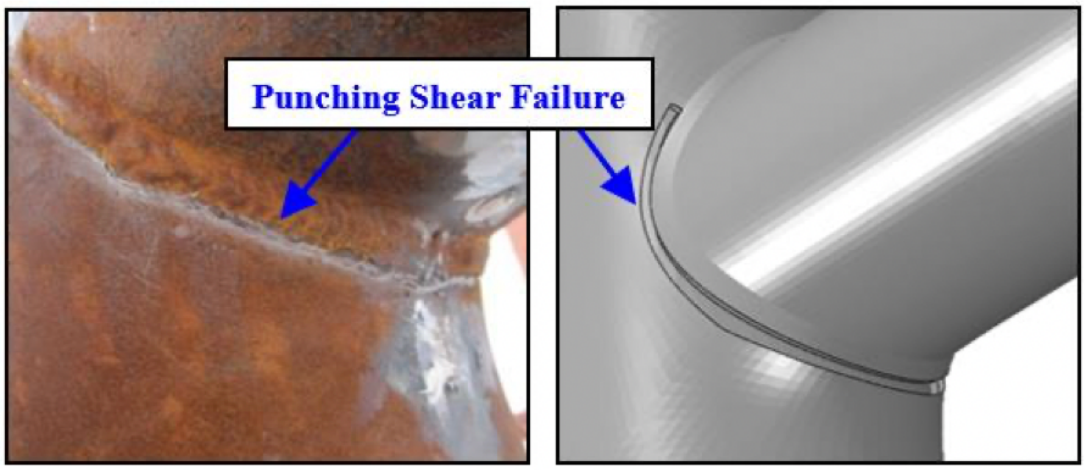

Figure 2.5: Example of Punching Shear Failure

2.6 Nonlinear Solution Settings

The numerical models developed in Abaqus, described in Sections 3.1 and 4.1, utilized material and geometric non-linear analysis techniques. Geometric non-linearity was included in the models to allow Abaqus to update the internal stiffness matrix at the end of each iteration to account for changes in geometry. The stiffness matrix in Abaqus can be updated due to changes in contact status and an increase in tensile forces, as is the case in large displacement analyses. Material non-linearity was defined by inputting plastic stress-strain data into the Abaqus material deck. Material non-linearity allows the connection to reach capacities past the yield point, redistribute internal forces, and eventually reach a rupture point that can be compared to experimental results.

The Newton-Raphson Solution Method was used to solve the non-linear model. This solution method is an iterative procedure, which works by first applying the total load to the model, then calculating initial displacement μ_i and then initial internal forces F_{int}. The stiffness matrix of the model is linearized for each step based on the current displacements, material properties, and contact status. Internal forces are calculated based on the strains in each element from the initial displacement and stiffness, using the formula $F = KX$. The internal forces are then used to find the current displacement increment $\Delta\mu^n = (F_{ext} - F_{int}^n)/K^n$. The residual force is then calculated by comparing the external and internal model forces; if the residual force is within convergence tolerance, the model converges; otherwise, another increment is calculated following the steps mentioned above.

A non-linear numerical analysis is performed by solving a sequence of discrete linear steps. At the end of each step, the model is updated, and the next linear step is performed. Due to the non-continuous nature of this solution, it is essential to correctly control the "time" or percentage of the analysis that is performed during each step. These steps can be controlled during analysis setup within Abaqus by setting initial, minimum, and maximum time steps. The analyses described in this Section utilized initial time steps of 0.1, minimum time steps of 0.0001, and maximum time steps of 0.2.

The General Contact feature in Abaqus was utilized to ensure contact was considered for all parts in the models. All default contact settings were utilized for General Contact, besides the tangential (friction) behavior, where a penalty factor of 0.5 was applied.

Chapter 3

Validation using Published Data

Experimental benchmarks were required to validate the finite element modeling methods utilized in this research program. To save fabrication and testing time the author used published experimental data to validate the numerical results reported herein.

3.1 Published Experimental Studies

To the author's knowledge, no publicly available studies contain data for non-planar connection geometries. However, published experimental data on planar HSS connections is still a useful benchmark that may be used to perform the initial calibration of numerical modeling procedures. The primary published experimental data used as a reference in this study was published by Bu and Packer in 2020 titled Chord End Distance Effect on HSS Connections [10]. In this study, planar T- connections were studied as shown in Figure 3.1. This referenced study posted experimental and numerical results for planar T-Connections, which included load-deformation curves. The study also published all its experimental inputs, such as material properties, engineering stress-strain data, finite element types used in numerical models, and all the measured experimental specimen dimensions. The level of detail provided in the referenced study made it ideal to use as a means for validation of numerical modeling methods used herein.

3.1.1 Numerical Model Setup

The author set up several numerical models in Abaqus to determine the model parameters that provide the best predictive capability in the ROFEMs. Key parameters were varied one at a time, and results were compared to the experimental results to determine which combination of parameters provided the most accurate prediction of the connection behavior. The primary model parameters studied were element type, size, and order, boundary conditions, and chord corner material properties. This sensitivity study was performed for the ROFEMs only as it is assumed that the default settings in IDEA StatiCa are conFigured to produce mesh-independent models. IDEA StatiCa also lacks a means of controlling other parameters, such as the extension of corner material properties.

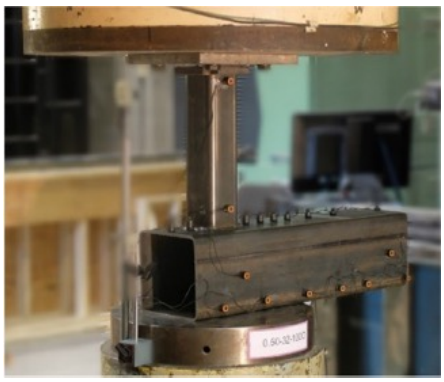

Figure 3.1: Uniplanar RHS Connection (Bu and Packer, 2020)

The data points used to determine the accuracy of each model were chord face deflection of 0.03*b_o and 5% plastic strain, as well as the onset of yield as determined by the stress-strain graph. The 3 percent chord face deflection and 5% plastic strain values are exact values output from each program; however, the onset of yield is approximate and is obtained by determining where the slope changes on the force-deflection curve. This value is used for reference only, while the other two quantities are used to show a percent difference between results from experiments and numerical models.

Abaqus models were set up as shown in Figure 3.2 and the IDEA StatiCa models were set up as shown in Figure 3.3. IDEA StatiCa models are set up by defining a connection type and specific member sizes and connection operations. Since IDEA StatiCa is a design program, member sizes were set to the nominal design dimensions from the AISC manual instead of the exact dimensions measured during fabrication. Fillet welds were similarly selected as the closest nominal size rather than an exact representation. These choices were made to show how accurate the program is when utilized as it would be by the typical

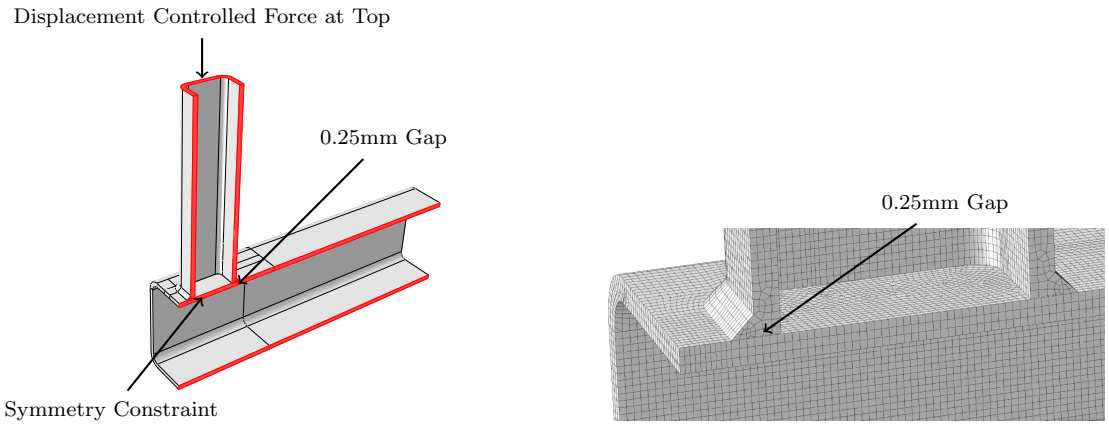

Figure 3.2: (a) Abaqus General Setup (b) Abaqus Weld Detail

designer. As seen in Figure 3.1 the main support for the test specimens is a circular load table under the bottom face of the HSS. To represent this load table, an end plate operation was used to connect the bottom of the HSS to a stiffening plate with a single bolt; the plate was in turn connected to a short post and grounded at its end. The single bolt connection allows the bearing plate to transfer bearing and lateral shear forces only, without preventing rotation of the chord face, closely resembling the actual contact between the tube and the table.

The shell models created in Abaqus were identical to the solid model shown in Figure 3.2, besides in the case of the weld representation. The fillet weld was explicitly modeled in the solid models, and a 0.25 mm gap was maintained between the branch end and chord face as shown in Figure 3.2(b). The gap was held to account for the possibility of the two members not being in contact while the joint was welded. In the shell model the branch was conservatively connected directly to the chord, without considering the increased shear perimeter created by the weld geoemetry.

3.1.2 Material Properties

Material stress-strain data was obtained directly from the published research. The referenced paper included engineering stress-strain data as well as coupon dimensions. The author

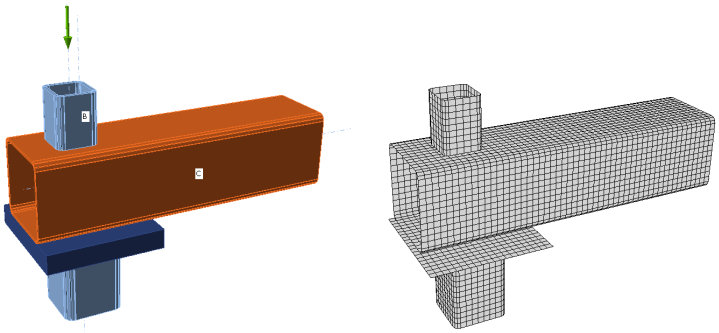

(a) (b)

Figure 3.3: (a) IDEA Statica Model Geometry (b) IDEA Statica Meshed Model

used the published stress-strain values to convert the data to true stress strain as seen in Section 3.1.2. IDEA StatiCa uses an elastoplastic material model, and thus the full stress-strain curve cannot be used. Instead, to stay consistent with the programs intended use the material properties for ASTM A500 Gr. C steel was used directly from the program's material library.

Conversion of Material Properties

The stress-strain values obtained during testing represent the engineering stress-stain values. Engineering stress-strain values do not accurately represent the uniaxial material properties, because they do not account for complex behavior of the tensile specimen during testing, such as reduction in area of the cross-section and development of multi-axial stress states. Before using this data in numerical models these phenomena must be considered and the data must be converted into what is known as true stress-strain values.

Engineering stress-strain can be characterized as having 3-4 distinct phases (i) a yielding phase (ii) a nonlinear elastic phase (iii) a hardening phase and (iv) a softening phase (otherwise known as necking). The difference in data is generally considered as negligible in phase (i), thus no conversion is required. The conversion in phase (ii) and (iii) is rather straight forward, as only minimal complex stress states have formed in the model. In these regions analytical approximations can be used as recommended by Callister [11].

$$\sigma_T = \sigma * (1 + \epsilon) \tag{3.1}$$

$$\epsilon_T = \ln * (1 + \epsilon) \tag{3.2}$$

In phase IV the tensile specimen develops complex triaxial stresses and non uniform deformations, which cannot be captured by the simplified equations presented previously. [24, 11, 46, 37]. Instead an iterative solution procedure must be used as recommended by Matic, Ling and Arasaratnam et al. [46, 38, 7]. Each of these research papers recommend an iterative solutions, which involve recreating the tensile coupons in a numerical model, converting stress-strain values by inserting an assummed constant into a recommended equation, solving the model, and then updating the constant depending on the outcome of the model. The most recent of these is the study performed by Arasaratnam et al., which built on the research performed by Matic and Ling. In this method the authors recommend the following process to convert engineering stress-strain data to true data.

1. Perform conversion in Phase (i), (ii), and (iii) using analytical approximations (see Figure 3.4)

2. Perform power regression on data in hardening region to determine a power law material constant, n (See Figure 3.5)

3. Perform conversion on data in hardening (Eq. 3.3) and necking region (Eq. 3.4) using weighted power law equations (See Figure 3.6):

$$F_t = F_{ut} * (\frac{\epsilon_t}{\epsilon_{ut}})^n \tag{3.3}$$

$$F_t = F_{ut} * [w * \frac{\epsilon_t}{\epsilon_{ut}}^n + (1 - w) * (1 + \epsilon_t - \epsilon_{ut})] \tag{3.4}$$

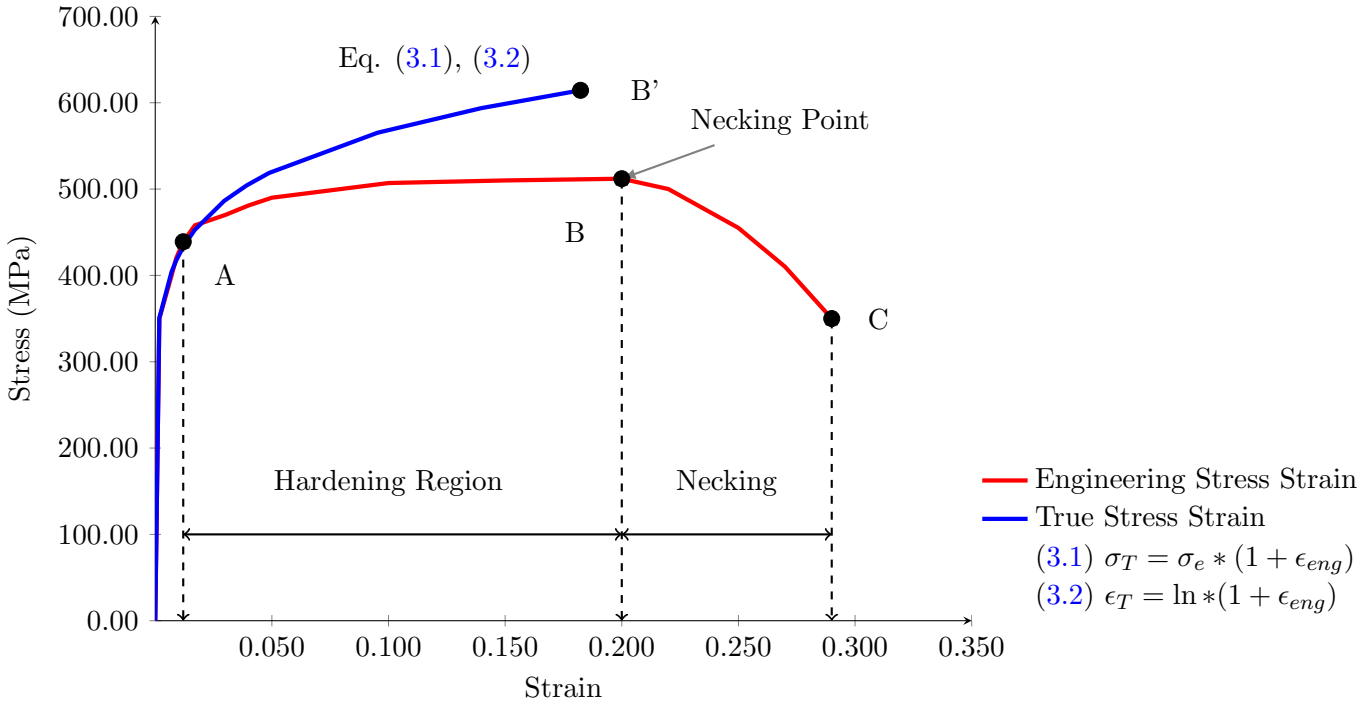

Figure 3.4: True Stress-Strain Conversion, Region ii

4. Insert converted data in numerical model of tensile coupon, solve model to determine match between numerical and experimental data

5. Adjust the power law constant (w) as required, repeat steps 3-5 (See Figure 3.7)

The results of the stress-strain conversion study performed herein can be seen in Figures 3.4, 3.5, 3.6, and 3.7).

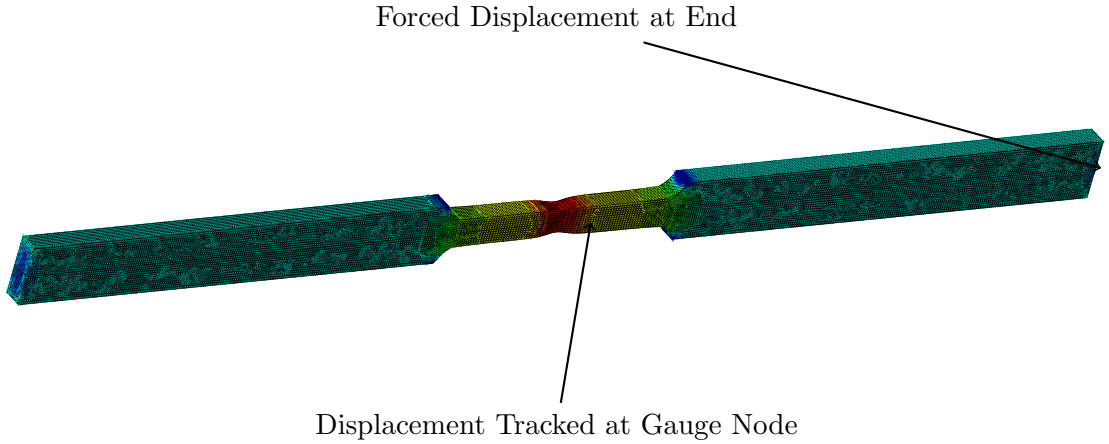

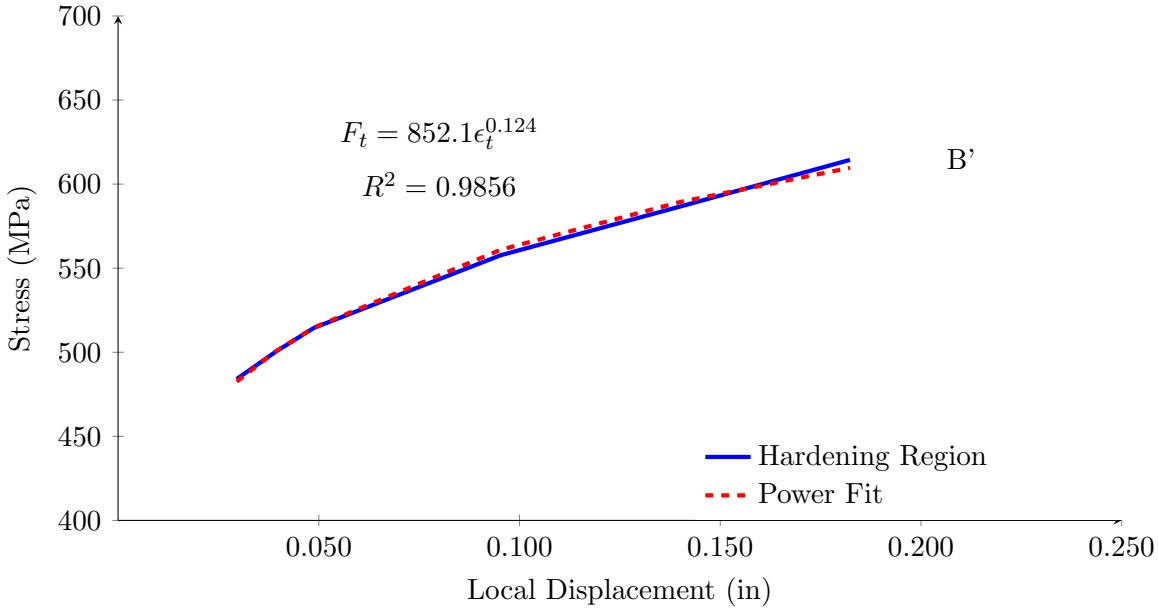

Figure 3.5: Power Regression of Hardening Region

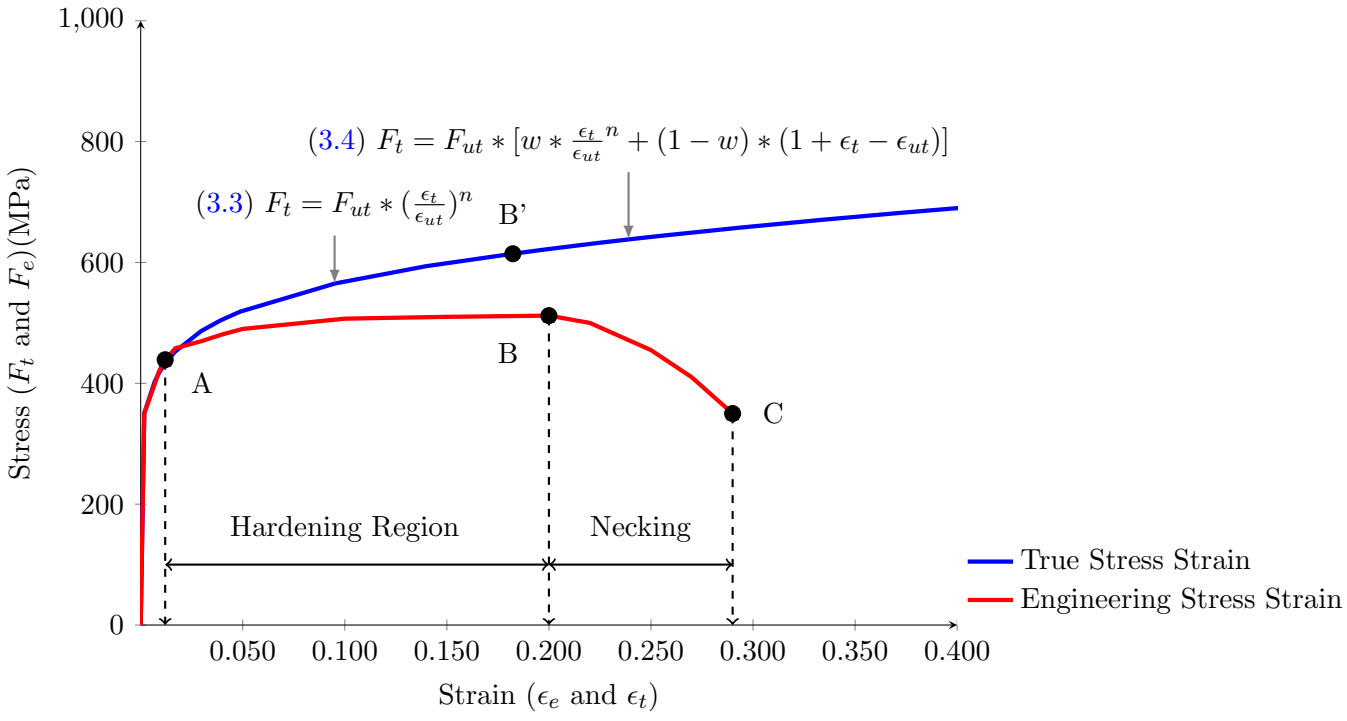

Figure 3.6: True Stress Strain Match

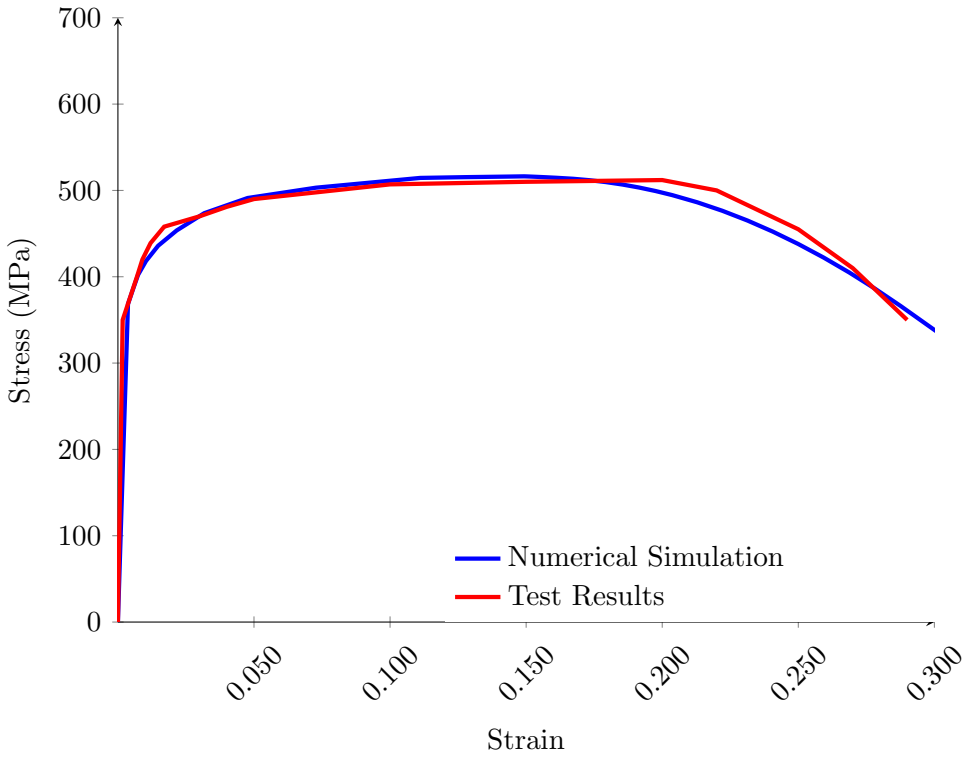

Figure 3.7: Numerical Model Engineering Stress-Strain Data Fit

3.1.3 Sensitivity Study

Numerical simulations are inexact and subject to uncertainty. The variable inputs into a numerical system may have small or large impacts on the mathematical output. To determine what inputs most affected the model results, a sensitivity study was performed, as shown herein and in Figure 3.8. The parameters studied included (i) Mesh size, (ii) number of elements through the thickness of the chord, (iii) boundary conditions, (iv) element type, and (v) chord corner material properties. The results shown follow the natural progression of the study. For example, when element type sensitivity was studied, the effects of strain hardening of the chord corners and contact between the table and bottom face of the chord were not included in the model. As each sensitivity study was completed, an optimal parameter was chosen and applied to the subsequent study until, eventually, the complete model setup was defined and the desired accuracy was achieved as shown in Section 3.1.3.

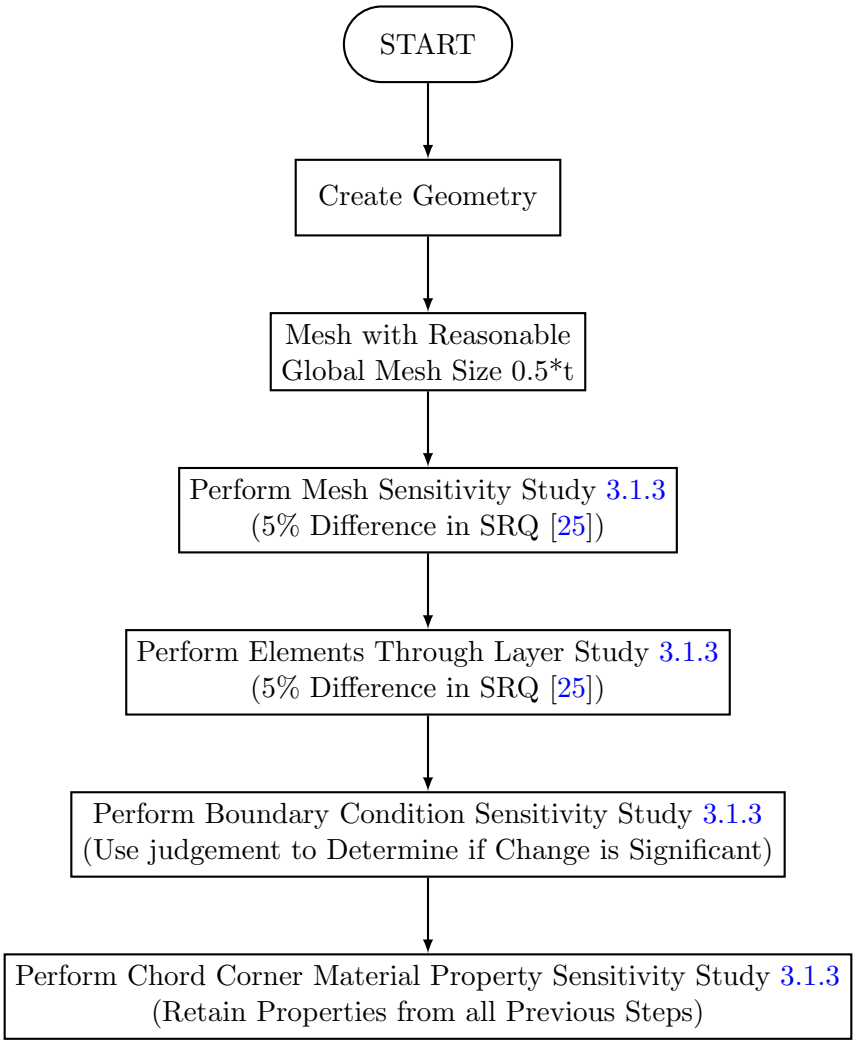

Figure 3.8: Sensitivity Analysis Process

Element Type

As described in Section 2.2 of this thesis, there are several element types used in finite element analysis. The performance of each element type depends on the type of phenomena being predicted. A parametric study was performed herein using different element types to mesh identical geometry. The results of the study were compared to the available experimental baseline to measure the accuracy of each element type.

As mentioned earlier, Abaqus offers a full suite of element types, but IDEA StatiCa offers linear quadrilateral plate elements only. Because of this, the element-type study was performed in Abaqus only. The first element types tested in Abaqus were solid elements. When using solid elements, TETs are generally thought to be a less efficient and less accurate element than HEXs, but can easily be used to mesh intricate geometry. This research aims to allow for a means to analyze non-planar HSS connected at any angle, which can lead to complex geometry at the joint. Meshing this geometry with HEX elements can become highly challenging, if not impossible. For this reason, it is desirable to show that TET elements can provide a similar level of accuracy.

Table 3.1: Sensitivity Analysis for Specimen X-0.5-21-25O (Mesh Size)

Mesh Size	Force at 3% Limit	Force at 5% Limit
2mm Tet	248	0.07
1mm Tet	233	0.09
0.5mm Tet	231	0.05

Figure 3.9 shows the force-displacement curve of each model meshed with varying element types, but identical mesh sizes, and compares those results to the experimental force-displacement result. Since, at this point, there are other model parameters that must be studied before determining the accuracy of individual components, it is not possible to report an exact percentage error for each element type. However, there does appear to be clear trends in the data that give the authors enough information to "select" an element type and continue with the sensitivity study. It is apparent from the results in Figure 3.9 that linear TET elements are far too stiff to be used in this application and will not be examined any further. Quadratic HEXs and Quadratic TETs both appear to yield reasonable results, with

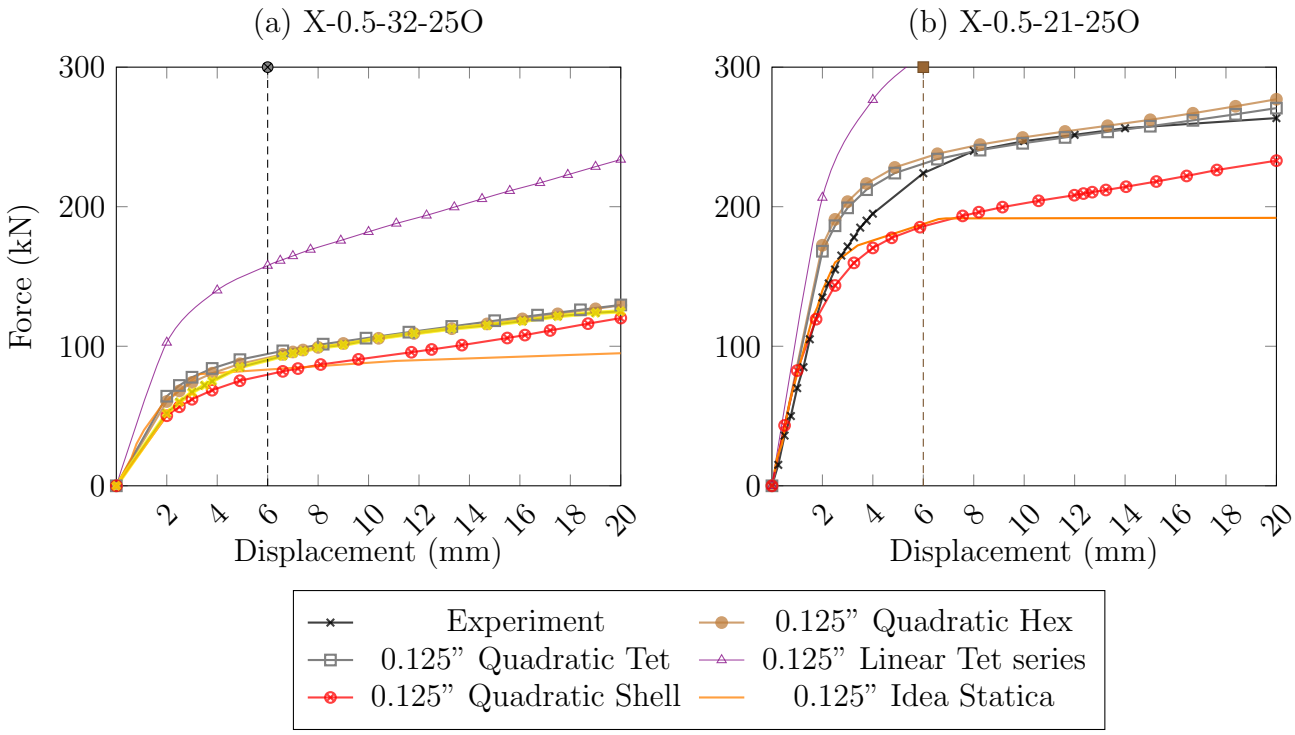

Figure 3.9: Element Type Comparisons - Force Displacement Curves

connection models meshed with TET elements being surprisingly slightly more flexible than the HEX models. Each of the shell models developed were more flexible than their solid counterparts, likely due to the reduced branch perimeter caused by ignoring the fillet weld geometry. In the remainder of the sensitivity study, quadratic TETs and HEXs will be used in each study.

Mesh Size

One of the most important procedures in the verification process is the mesh refinement study. As stated previously in this thesis, a numerical model is a mathematical approximation of a physical system. The model, as an approximation, has intrinsic sources of error, one of which is the mesh discretization error. When acted on by an outside force, a structure will take a deformed shape with the lowest possible energy while obeying the laws of compatibility and continuity. The potential energy of a finite element model can be represented by the following formula:

$$U = \frac{1}{2} * \int_V \sigma_h^t * \epsilon_h dV \tag{3.5}$$

Notice that this formula's stress and strain variables are proportional to the displacement term. It must then be understood that a numerical model is, in normal circumstances, consistently stiffer than the physical model. This can be intuitively understood if one pictures a cantilevered beam, loaded at its end and represented by an increasing number of linear elements. As the number of elements increases, the displacement along the beam will become smoother, and the displacement at the tip of the beam will increase. The behavior of more complex models behave similarly to this simplified model. Inexact formulations of a numerical model introduce errors, which cause the results to be farther from the exact or minimum potential energy (MPE) solution. As the mesh size (grid) is reduced, the numerical model solutions will tend towards the upper bound of the MPE solution.

The concept of mesh refinement is commonly used in practical design applications, with many designers opting to check the effect of mesh size on numerical models by solving the model several times with decreasing mesh size of $h_{-1}/2$, with h_{-1} representing the mesh size of the previous solution. The System Response Quantity (SRQ) is then checked at a critical location for each mesh size and compared to the previous. In this process, a mesh grid is considered converged when the SRQ of two consecutive solutions are within 5% of one another. This procedure can be found in multiple textbooks and the user manuals of some of the most popular FEA programs [5, 57].

In this thesis, a more specific convergence method was desired. The convergence criteria used herein is an adaptation of the Grid Convergence Index (GCI), as suggested by Kwaśniewski. The GCI is a discretization error indicator primarily used in CFD but can easily be adapted for use in solid structural mechanic FEA models [56, 36]. The GCI index is developed based on the understanding that most models, complex enough to require FEA, do not have an exact analytical solution. For this reason, a "Posteriori" approach is needed, meaning mesh convergence must be determined based on repeated solutions of the model [36].

The ultimate indicator of convergence in this method is the GCI itself:

$$GCI = \frac{F_s|\varepsilon|}{r^p - 1}100\% \tag{3.6}$$

where P is the order of convergence defined by:

$$p = \frac{\ln\left(\frac{f_3 - f_2}{f_2 - f_1}\right)}{\ln(r)} \tag{3.7}$$

f_i is the SRQ value for each trial, r is the refinement ratio, or the amount the mesh size is reduced each successive trial. F_s is a factor of safety set based on results in CFD calculations [53], which represents a 95% confidence that the solution is within +/- the percent deviation described by Eq. 3.6. ϵ is simply the relative difference between subsequent solutions, as follows:

$$\varepsilon = \frac{f_1 - f_2}{f_1} \tag{3.8}$$

It is a requirement of the GCI that the values considered be in the asymptotic range, which is confirmed by Eq. 3.10. The result of this equation will not be exact, but a result within 1% is thought to be well within the range of convergence [1, 53, 36].

Finally, the asymptotic value can be predicted with Eq. 3.9.

$$f_{h=0} \cong f_1 + \frac{f_1 - f_2}{r^p - 1} \tag{3.9}$$

Table 3.2: GCI Results - Plastic Strain Convergence

Element Type	**Mesh Size**	**Force at 5%-Strain**	ϵ 3.8	**P** 3.7	GCI_{12} 3.6	GCI_{23} 3.6	**Check** 3.10	**f** 3.9
C3D8R	0.5	235.52	-	4.69	4.39E-04	0.0112	0.99279	235.446
	1	237.23	-0.007					
	2	281.39	-0.186					
C3D10	0.5	236.35	-	4.63	5.03E-04	0.0124	0.99207	236.27
	1	238.24	-0.008					
	2	285.20	-0.197					

$$GCI_{23} = r^p * GCI_{12} \tag{3.10}$$

The GCI method was used to demonstrate that the results of the numerical models described in this section are independent of mesh density. Three mesh sizes of 2mm, 1mm, and 0.5mm were considered, as seen in Figure 3.10. The results of the mesh convergence study performed herein can be seen in Figure 3.11 and Table 3.2. A cursory look at Figure 3.11 suggests that a mesh size of 2mm tends to create an artificially stiff model, whereas a mesh size of 1mm and 0.5mm tends to represent the model prediction reasonably well, compared to the experimental results. In this case, since there are other sources of errors in the model (boundary conditions, material properties, etc.), the relative prediction between experimental and numerical results cannot be used as a reliable predictor. Instead, the Posteriori approach of the GCI index must be strictly adhered to.

Table 3.2 shows the results of the Grid Convergence Index. Column one of this table indicates that a convergence study was performed for two mesh types, quadratic TETs (C3D10) and quadratic HEXs (C3D8R). The second column shows the mesh density of each solution, and column 3 shows the force applied to the model to cause a 5% plastic strain at a critical location, a distance of 0.5*t from the weld toe. Note that this value decreases as the SRQ converges to the asymptotic solution. This is analogous to the stress increasing in a model during convergence and demonstrates failure at a lower applied load. The mesh densities considered produced asymptotic range values of 0.99279 and 0.99207 for the HEX and TET meshed model, respectively, showing that all sizes are in the asymptotic range.

The converged solutions for both element types are similar at 235.446 kips and 236.72 kips, respectively. An element size of 0.5mm is proven to create a mesh-independent solution and will be utilized for the remainder of this sensitivity study.

Number of Elements Through the Thickness

Failure of an RHS connection may be controlled by bending of the chord face. In bending dominant problems, the stress through the cross-section is non-linear; thus, to properly analyze the response of a solid in bending, several elements must be used through the layer. The decision was made in this study not to perform an explicit element through the thickness sensitivity study. Instead, it can be observed that the element size sensitivity study also captures the effects of elements through the thickness as the 2mm mesh model contains one element through the thickness, the 1mm mesh model contains two elements through the thickness, and the 0.5mm mesh model contains three elements through the thickness. Mesh size, not layers, will be the controlling consideration when meshing the models in the subsequent steps of the sensitivity study.

Boundary Conditions

The next parameter considered in the sensitivity study was the boundary condition set. There were a few necessary boundary conditions in this model. The model was created using

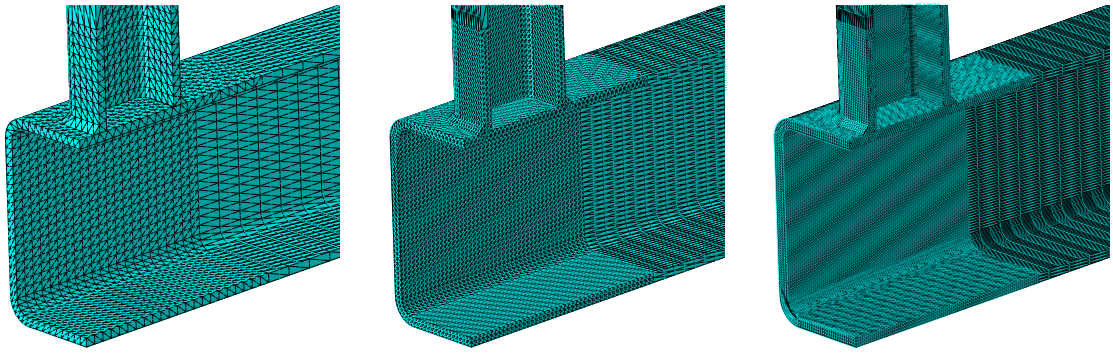

(a) (b) (c)

Figure 3.10: (a) 2mm mesh (b) 1mm mesh (c) 0.5mm mesh

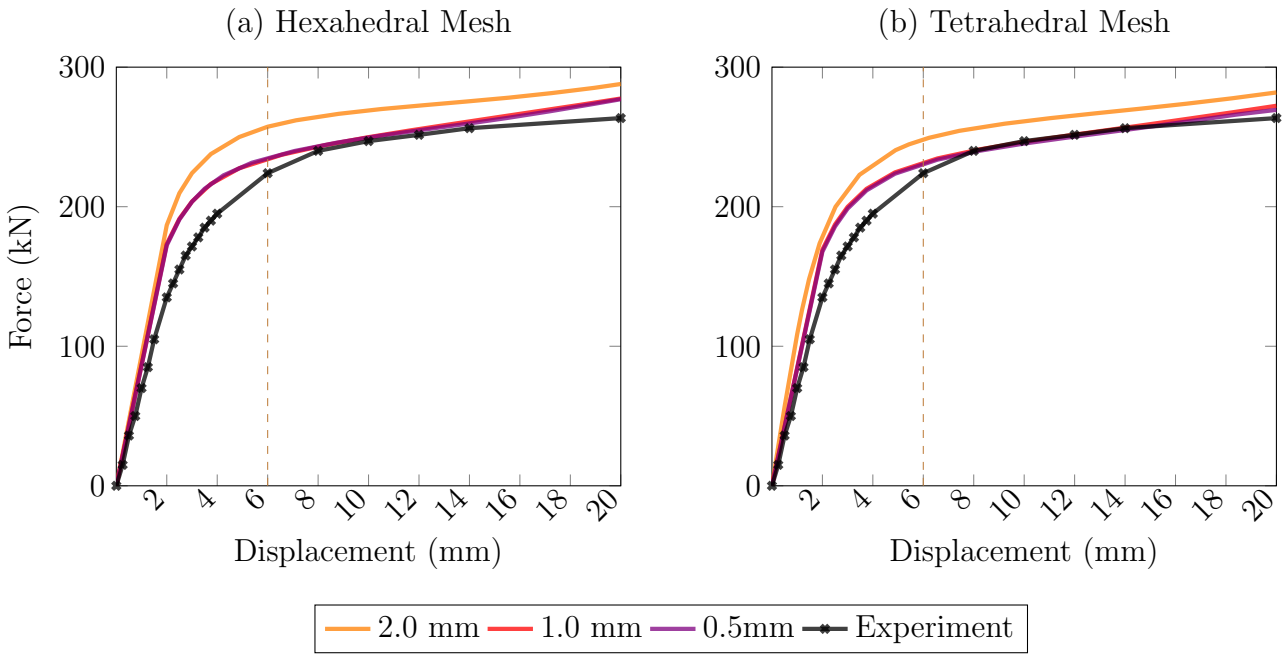

Figure 3.11: X-0.5-21-25O Element Size Sensitivity Study

half symmetry, so a symmetric constraint was placed on the cut portion of the model as seen in Figure 3.2. The experimental specimen was also loaded at the top of the branch, as seen in Figure 3.1. To simulate the controlled force application of the actuator, a displacement constraint was placed on the top surface of the branch via a single loading node at the branch corner and an equation constraint was used to tie all other nodes on the surface to the singular loading node.

The author examined the boundary conditions at the symmetry plane and actuator and determined there was no opportunity to vary their application. However, the author determined that there were multiple viable ways to model the support condition between the bottom face of the chord and the loading table. The two methods of modeling this support chosen were (i) placing a displacement constraint on the bottom face of the chord and (ii) adding a plate under the bottom chord face as well as a contact interaction between the face and the chord to represent the contact between the chord and loading table in the experiment. The major difference between the two methods is that the second method will allow the chord face to separate from the loading table, likely simulating the real life scenario more closely.

Table 3.3: Effects of Boundary Condition Study

	Null Boundary Constraint	Contact Boundary Condition	Experiment
Force at 3% Deflection	235 kip	219.17 kip	224 kip
Percent Difference to Experiment	4.74%	2.25%	-

The resulting displaced shapes can be seen in Figure 3.12. As can be seen in this Figure, it is clear that the bottom chord face does tend to bend and separate from the loading table; even though the global loading is purely compressive, the top chord face bends under the load and, in turn, bends the chord wall out and the chord bottom face up. Since the first modeling method limits the overall bending of the chord shape, it is logical that it also adds stiffness to the overall connection.

In the experimental study, the T-branch connections, as seen in Figure 3.1, were loaded by a hydraulic actuator at the top of the chord and supported by a reaction table at the bottom face of the chord. In the sensitivity study presented herein, the top of the branch was consistently loaded evenly, and the specimens were cut in half and constrained by symmetry constraints, as can be seen in Figure 3.2. The support condition at the bottom face of the chord was varied between a simple null vertical displacement constraint and a contact condition between the chord and a solid block of steel. The effect that each of these boundary conditions have on the model results can be seen in Table 3.3. As can be seen in the table, adding contact between the chord and loading table significantly reduced the stiffness of the connection, reducing the over-prediction of load at 3% deflection from a value of 4.74% to 2.25%. In fact, this change increased the flexibility of the connection so much that the numerical model appears to under-predict the capacity of the connection in much of the non-linear region. This is likely because the strain hardening of the chord corner is not yet included in the model, which will be discussed in Section 3.1.3.

Chord Corner Material Properties

Hollow structural sections (HSS) are formed by either hot forming or cold rolling. Hot-formed HSS have superior mechanical properties but are not commonly available, mainly due to the elevated fabrication price. Most of the HSS fabricated in North America is

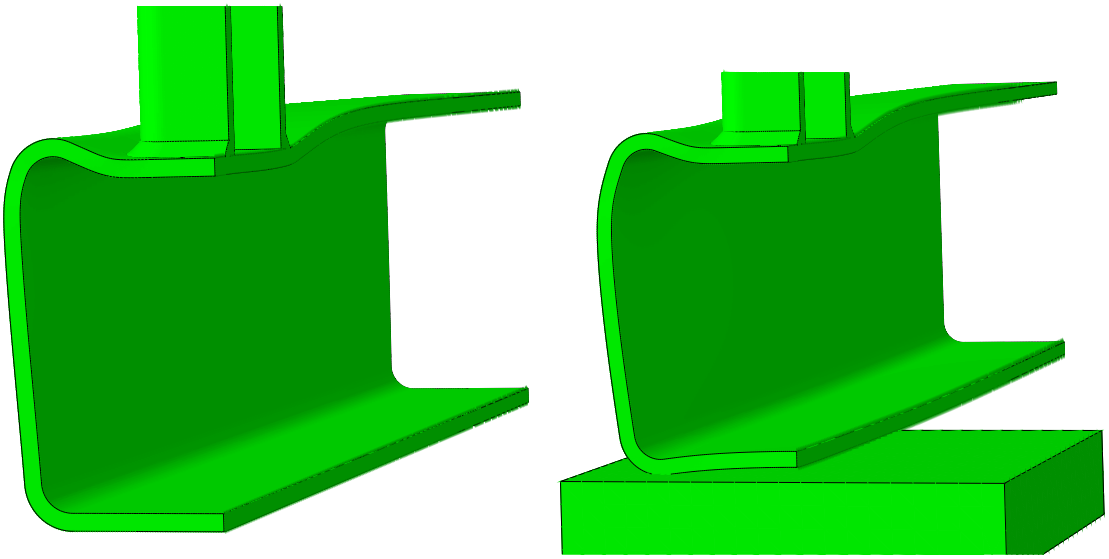

(a) (b)

Figure 3.12: (i) Fixed Constraint (ii) Contact with Load Table

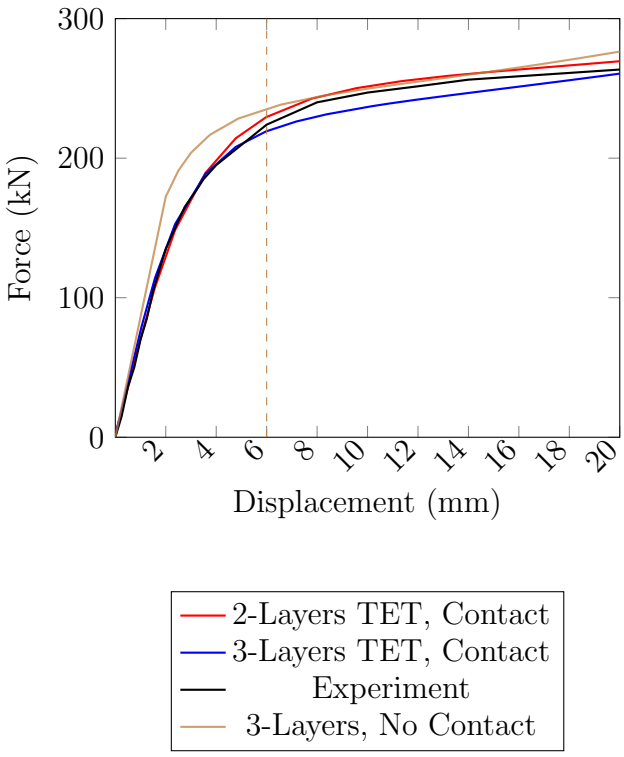

Figure 3.13: X-0.5-21-25O Boundary Condition Sensitivity Study

cold formed. The cold-forming process increases the material's ultimate and yield strength, decreases ductility, and increases stiffness. These changes in material properties are most significant at the corners but gradually extend into the flat portions of the HSS, which can significantly alter the overall mechanical properties of the tube [58], [3].

The severity of the change in mechanical properties largely depends on the fabrication type. As described in Sun's 2014 paper titled Mechanical Behaviour of Cold-Formed Hollow Structural Section Material, there are two main methods to cold form HSS utilized in North America [58]. The first method is direct forming. In this method, flat coils of steel are directly rolled into an open shape and welded at a seam, as seen in Figure 3.14. The second method used is called continuous forming. In this method, flat steel coils are rolled into a circular open section, welded at a seam where the two rolled sides meet, and then the circular walls are flattened into the correct shape, as seen in Figure 3.15.

The chord corner material properties used in this numerical model are taken directly from material testing by Fan et al. during experimental testing [27]. The referenced testing includes material properties from coupons cut at the corners and the flats. However, there were not enough coupons taken to determine exactly where the increase in yield stops in the flat section. A sensitivity study was performed to determine the extension of the corner material that provides the most accurate results. In this sensitivity study, the corner material properties were applied to the corners only or extended a distance of $0.5*\pi*r_i$ into the flat sections as recommended by [3]. In this study, the remaining flat material properties were kept the same as the virgin sheet metal.

The results of this sensitivity study can be seen in 3.16. The numerical model used for this sensitivity study included each of the modeling parameters presented throughout Section 3.1 that created the most accurate results in the respective sensitivity studies. The model was made using quadratic TET elements, with a mesh size of 0.5mm, at least three elements through the thickness, and contact type boundary conditions at the bottom chord. It can be seen in this graph that, in this case, extending the corner material properties a distance of $0.5*\pi**r_i$ provides results that most closely match the results of the physical tests.

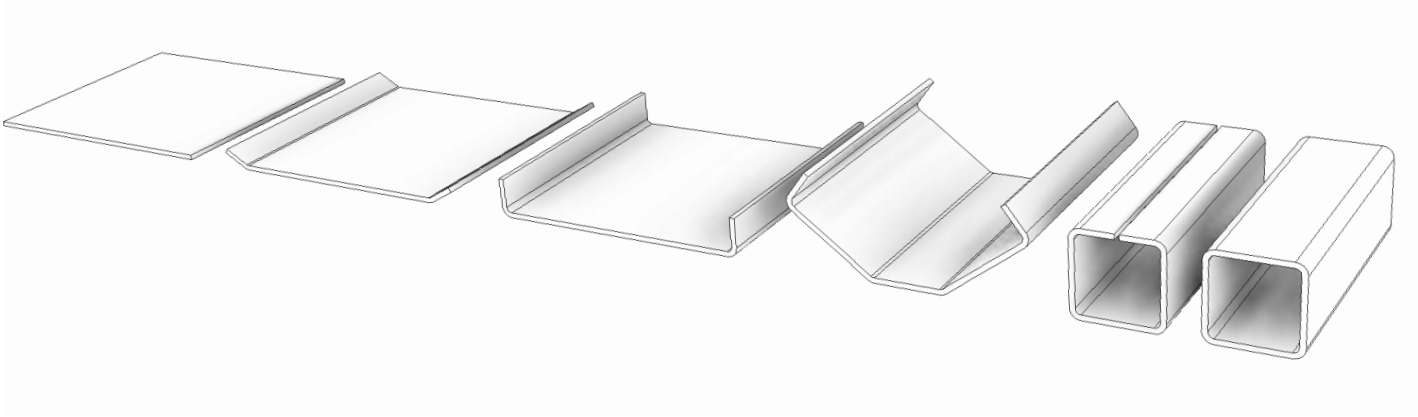

Figure 3.14: Direct Forming Process

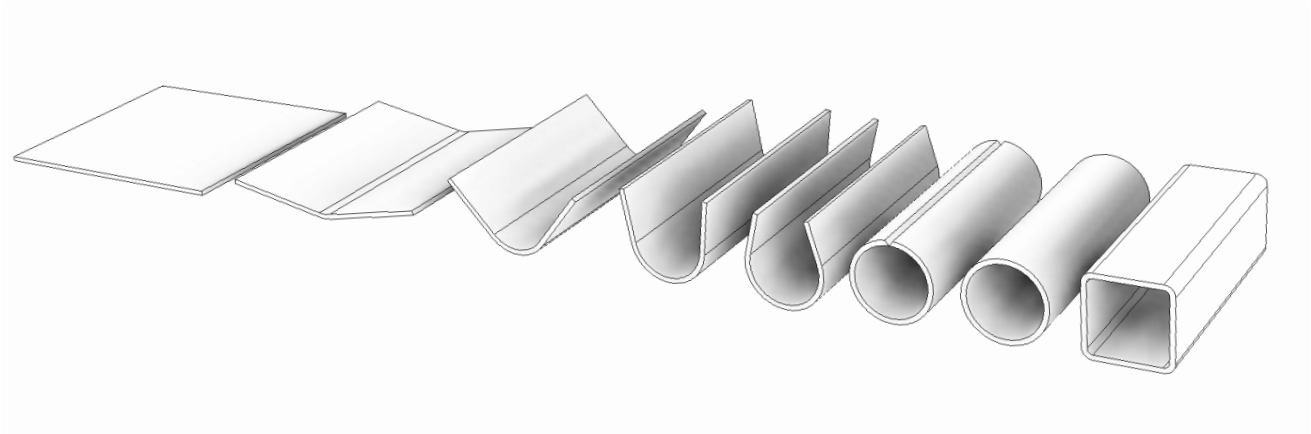

Figure 3.15: Continuous Forming Process

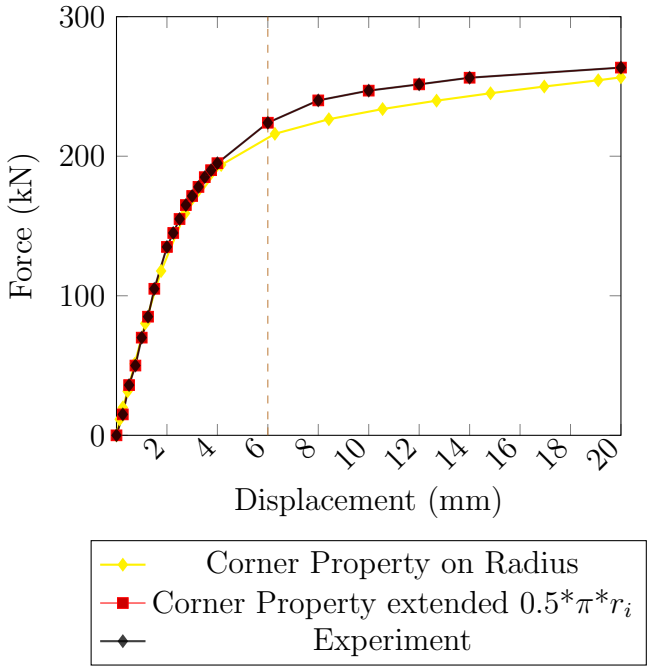

Figure 3.16: X-0.5-21-25O Corner Material Property Sensitivity Study

Results of Sensitivity Study

Based on the results of the sensitivity study performed the following model parameters were chosen:

(i) Mesh Type - Quadratic Tetrahedral

(ii) Mesh Size - 0.5mm

(iii) Mesh Layers - 3 Layers Minimum

(iv) Boundary Conditions - Contact at Load Table

(v) Chord Corner Material Properties - Properties Extend 0.5*π*r_i

The resultant force-displacement graphs developed from models using all of the above parameters are shown in Figure 3.17. It can be seen in these Figures that the numerical models created with the parameters described in this Section accurately predict the behavior of connections X-05-21-25O and X-05-32-100O. Using 3% local deformation as the relevant

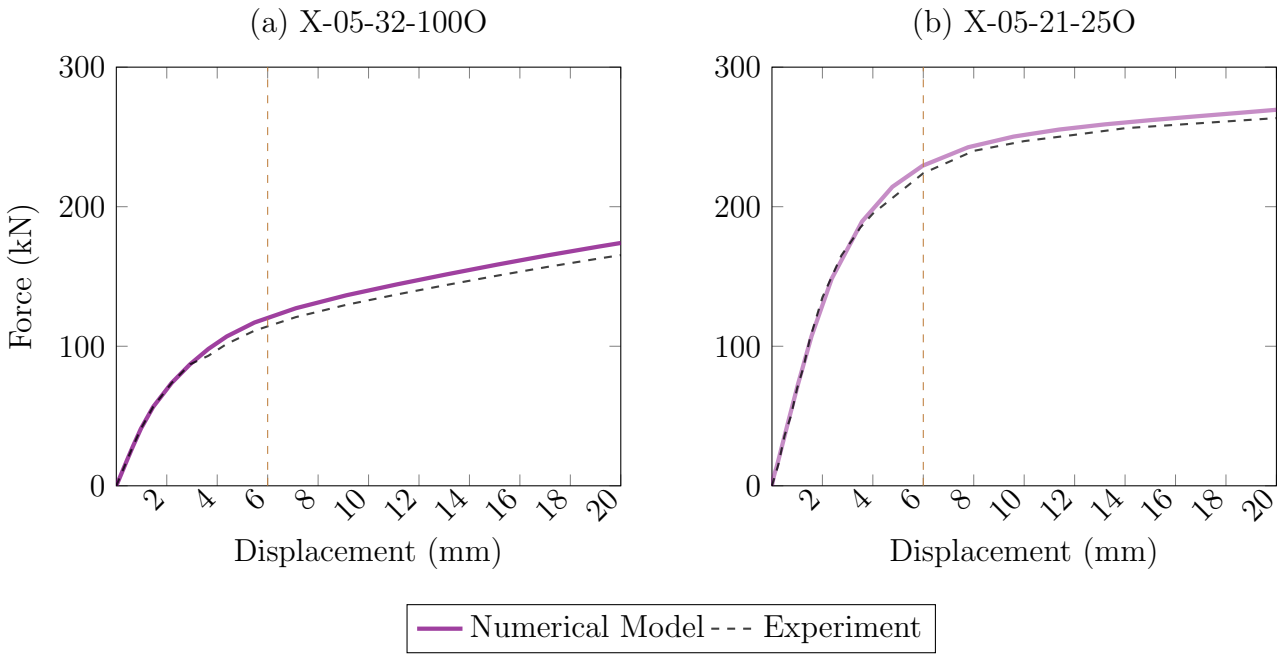

Figure 3.17: Model Results with Results of Sensitivity Study Incorporated

SRQ, the numerical models have a 5.26% and 2.32% error, respectively, compared to the experimental data.

3.1.4 Results

The results for the planar connections studied in this Chapter can be seen in Figure 3.18. As seen in this Figure, the calibrated Abaqus models accurately predict connection stiffness in the linear region. The models appear to slightly over-predict connection stiffness in the non-linear range. The Abaqus model of the X-05-32-100O specimen reached 3% local deformation at a 5.26% higher force than the experimental specimen. The Abaqus model of the X-05-21-25O specimen reached 3% local deformation at a 2.32% higher force than the experimental specimen.

The DOFEM created in IDEA StatiCa also accurately predicted connection stiffness in the linear region, as shown in Figure 3.18. However, as expected, the IDEA StatiCa model was significantly more flexible than the experimental model in the non-linear region. The IDEA StatiCa model of the X-05-32-100O model was 14.2% more flexible at 3% local

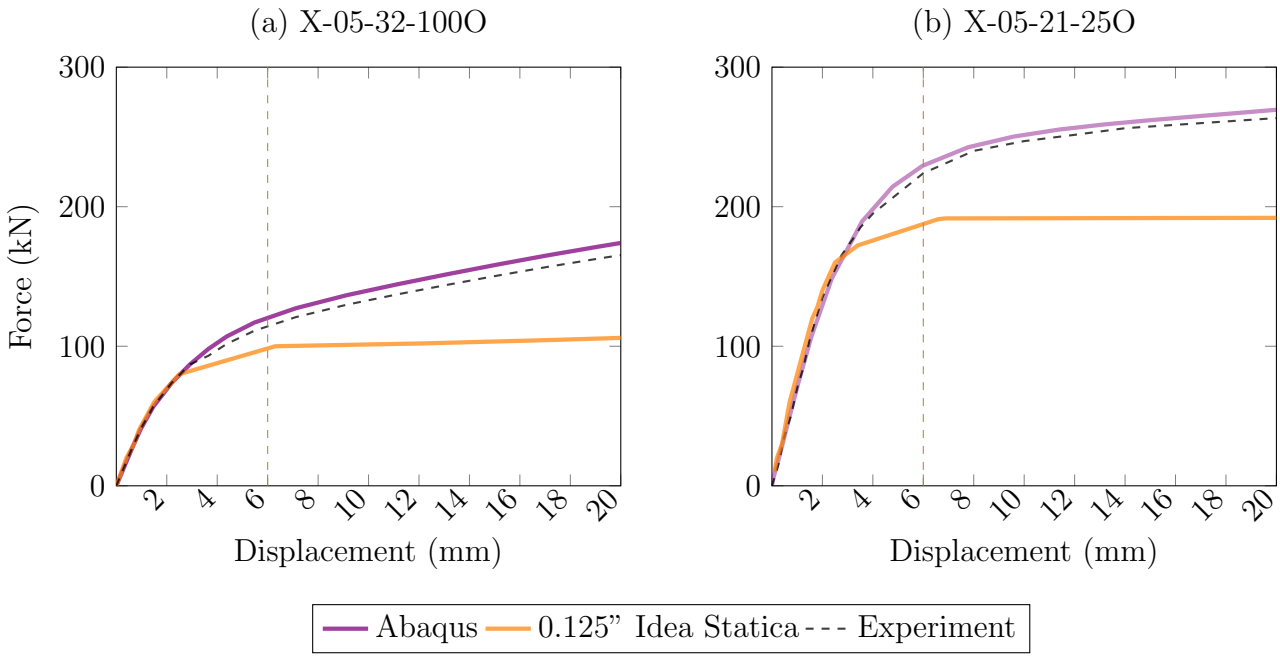

Figure 3.18: Planar Connection Results

deflection, and the IDEA, StatiCa model of the X-05-21-25O model, was 22.5% more flexible than the experimental model. It was expected that the IDEA StatiCa model would be more flexible than the experimental and research-oriented finite element models in the non-linear region because the IDEA StatiCa material model does not include strain-hardening effects.

These results show that, if properly calibrated, a research-oriented finite element tool such as Abaqus can be used to predict the behavior of HSS connections accurately. These results also show that IDEA StatiCa can be used as a conservative design tool for HSS connections. IDEA StatiCa's ability to predict connection force distribution using Finite Element Analysis may help a designer determine the capacity of general connection types where empirical equations are unavailable.

Chapter 4

Validation Using Experimental Data

4.1 Bird Beak Connections

The available published experimental data, although useful, is limited to planar connection geometry. The author acknowledges that it is possible that there are relevant phenomena associated with non-planar connections that are not captured in the experimental tests of planar connections. However, performing experimental studies of non-planar connections would require a custom testing apparatus and may be prohibitively expensive for most researchers. Instead, to vary the geometry and still create a connection that can be reasonably validated with experimental specimens, the author created numerical models of bird beak connections. To create these connections, the chord was rotated 45 degrees, which made the branch connect at the corner of the chord. This connection is more similar to the non-planar connections because it results in a non-uniform internal force distribution concentrated at the chord corner rather than at the flat face and creates a more complex weld, which cannot be easily fillet welded on all sides. Research-oriented models created in Abaqus and modeled using the parameters calibrated in the previous chapter will be used to extend the research program that was started in Chapter 3. The results of these numerical models will be compared to (1) the controlling strength of the planar analogue connection as determined by the available AISC equations for planar RHS connections and (2) the strength of the connections

as determined by the Design Oriented Finite Element Modeling program Idea StatiCa.

4.2 Prototype Geometry

To encourage future experimental testing and validation of the numerical results in this Section the models were built to match a particular prototypical geometry. Drawings of this geometry can be seen in Appendix A. These drawings show that the geometry should be built with HSS 4x4x$\frac{1}{4}$ chords and HSS3x3x$\frac{1}{4}$ branches. An HSS3$\frac{1}{2}$x3$\frac{1}{2}$x$\frac{1}{4}$ should be inserted inside the branch as a backer sleeve to make a Complete Joint Penetration (CJP) weld. The author has opted to specify a CJP weld due to its ability to accommodate general connection geometries. A fillet weld could be made all the way around this connection using the AWS D1.1 pre-qualified weld detail; however, at excessive dihedral angles, the amount of filler metal required to match the strength of the tube is excessive. A partial joint penetration groove weld could not be made for this connection. According to AWS D1.1, to create a PJP weld, the base metal must be at least 7/16" thick, and the root face must be at least 1/4" thick. Since the branch is only 1/4" thick, this weld can not be made.

Two types of bird beak connections were studied in this Section. The first type of specimen was an X-connection with a branch connected on either side of the chord. The other was a T-connection with a branch connected at the top only. The X-connections bottom branch will be bolted to a reaction table, while the top branch will be bolted to a hydraulic actuator. The T-connections chord will be supported at its ends by 1 1/2" pins, and the branch will be connected at its top end to the hydraulic actuator. The T-connection model was developed to allow some flexural stress to develop in the chord near the branch-chord joint, while the X-connection created local forces only.

4.2.1 Material Properties

Non-linear material properties obtained from the published research seen in Chapter 3 were used for all parts of the models described in this Section. Material data was not directly

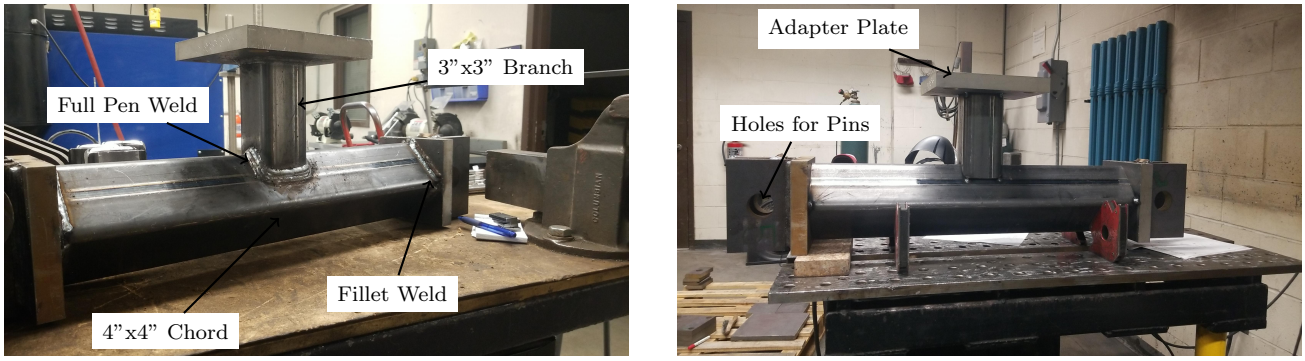

Figure 4.1: (a)T-Specimen Welds (b)T-Specimen Setup

measured for chord corners, branches, bolts, or plates. Instead, chord corner material properties were estimated per the guidance discussed in Section 3.1.3, and branches, bolts, and plates were assigned the same material properties as the chord flats. The plates and bolts in the connection did not experience any stresses above their respective yielding points. The constant stress-strain rate prior to yielding, Young's Modulus, is essentially identical in all grades of mild carbon steel; therefore, it is unlikely that this simplification introduced significant error into the model.

4.3 Numerical Models Setup

Numerical models were created for each test specimen in Abaqus and IDEA StatiCa. Initial model parameters were set from the results of the Bu and Packer verification study shown in Chapter 3, this mainly applied to the Abaqus model. The key features of each model are shown in the following sections.

4.3.1 IDEA StatiCa X-specimen

The X-specimen Design Oriented Finite Element Model (DOFEM) was created in IDEA StatiCa Connection only and not IDEA Member. As explained in Section 2.4 IDEA Member is a program that allows the user to model full-length members with multiple connections. Alternately, IDEA Connection is a program that allows a user to model only partial length

members with a single connection. IDEA Connection enables the user to analyze a single connection without explicitly including entire members by automatically cutting the primary member at a distance away from the center of the joint and applying a super element to the center and ends of the connection as explained in Section 2.4. The joint is then loaded by either (1) applying moments and shears to the ends of the connection to create accurate internal forces at the center nodes or (2) applying a force at the top of the branch. Since the X-Specimen is not connected at the chord ends and load is transferred directly from the top branch through the chord to the bottom branch an IDEA Member model would not likely provide a significantly different solution than the IDEA Connection model.

IDEA Connection

The IDEA Connection Model can be seen in Figure 4.2. In this model, the maximum mesh size was set to 0.1 inches and the maximum number of iterations was set to 100. Allowable Strength Design criteria were used for code calculations, but all safety factors were set to 1.0 for easier comparison to experimental and Research Oriented Finite Element Model results. The limiting plastic strain was set to 15% to allow the solution to run after code-based failure.

To obtain the load-displacement curve and displacement at 5% plastic strain the model was supported at the bottom branch and loaded with increasing axial loads at the top branch. The author edited the program's configuration file to show global displacements in the model; plastic strains and local deformations are shown by default. IDEA Connection does not offer a way to graph the force-displacement behavior of a connection, but the author was able to run multiple solutions and record the force and displacement of each in order to manually create a graph.

4.3.2 Abaqus X-Specimen

The X-Specimen Research Oriented Finite Element Model (ROFEM) was modeled as a solid with three planes of symmetry as seen in Figure 4.4. The experimental joints were made

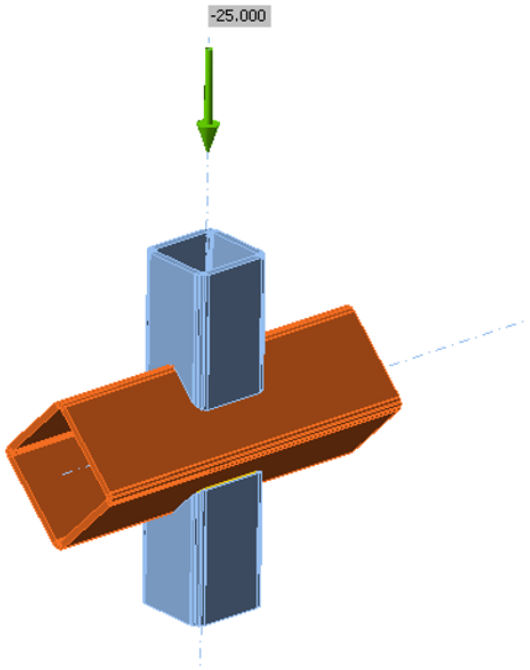

Figure 4.2: Idea Statica X-Specimen Isometric

with Complete Joint Penetration welds with a smaller width HSS used as a backer sleeve. To represent this in the numerical models two separate models were created. Both models were made with the chord and branch being one solid with continuous mesh to represent the complete fusion of the two members, but one of the models included the thickness of the sleeve in the branch and one did not include the sleeve as shown in Figure 4.5. Results from both models can be seen in Figure 4.3. This graph shows that the inclusion of the backer does not significantly affect the flexibility of the connection.

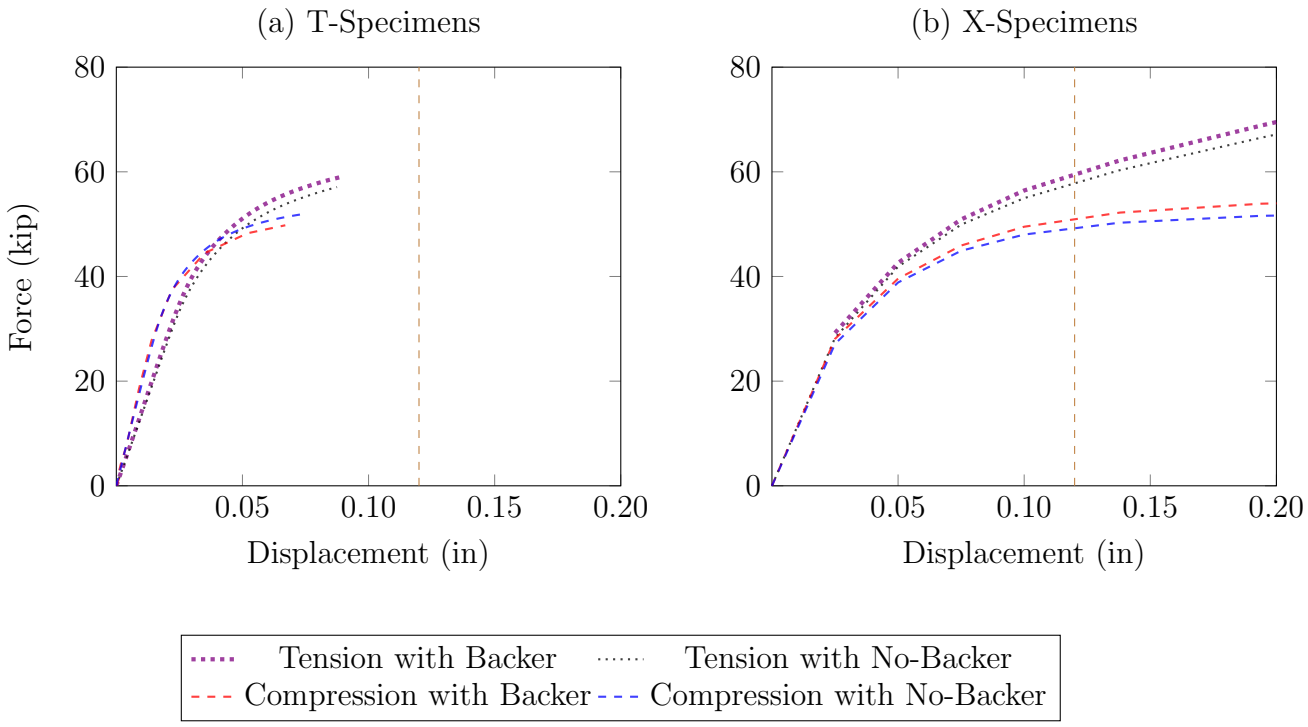

Figure 4.3: Backer Sensitivity Study

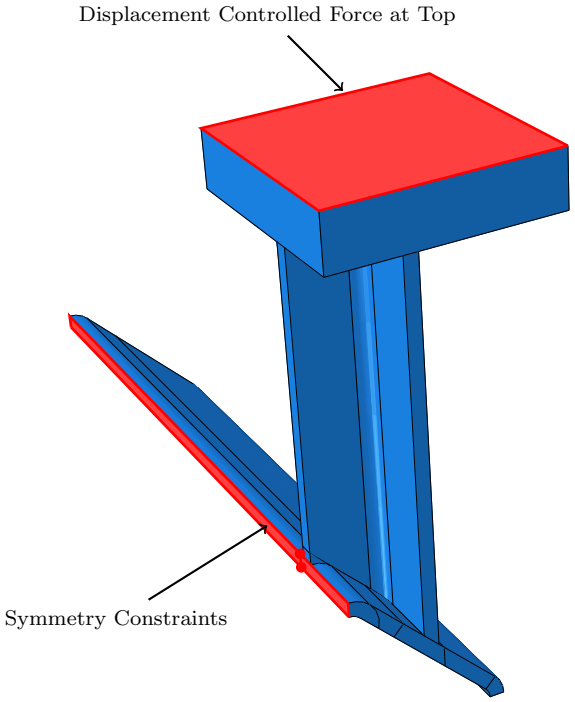

Figure 4.4: T-specimen Branch-Chord Mesh

These models were meshed with the automatic mesh feature in Abaqus using 10-sided quadratic TET elements. A global mesh size constraint of 0.1-inches was applied to the model and a minimum number of elements was set to 3, for the curves that represented the "through-thickness" portion of the HSS, per the results of Chapter 3.

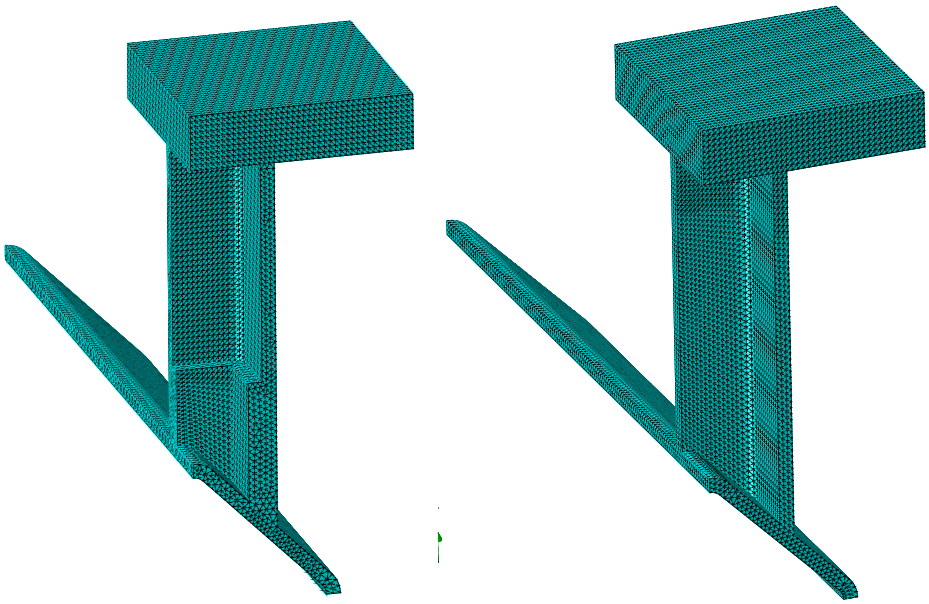

(a) a (b) b

Figure 4.5: (a) X-Specimen Thickened Branch (b) X-Specimen Nominal Branch

As stated previously, these numerical models took advantage of symmetry and allowed the author to create quarter-sized models. Symmetry constraints were applied to each plane of symmetry to fully constrain the model, no additional constraints were required.

These models were loaded with a displacement-controlled force of 0.4-inches on a single node, called the "loading node", which sat on the corner of the top surface of the loading plate. This load was linked to all other nodes on the top surface of the loading plate with a coupling equation, U1-U2=0, where U1 is the loading node and U2 represents all other nodes on the top surface. The displacement-controlled loading was initiated in the first loading step, with no additional steps needed for contact initialization. No contacts were assigned for this simulation.

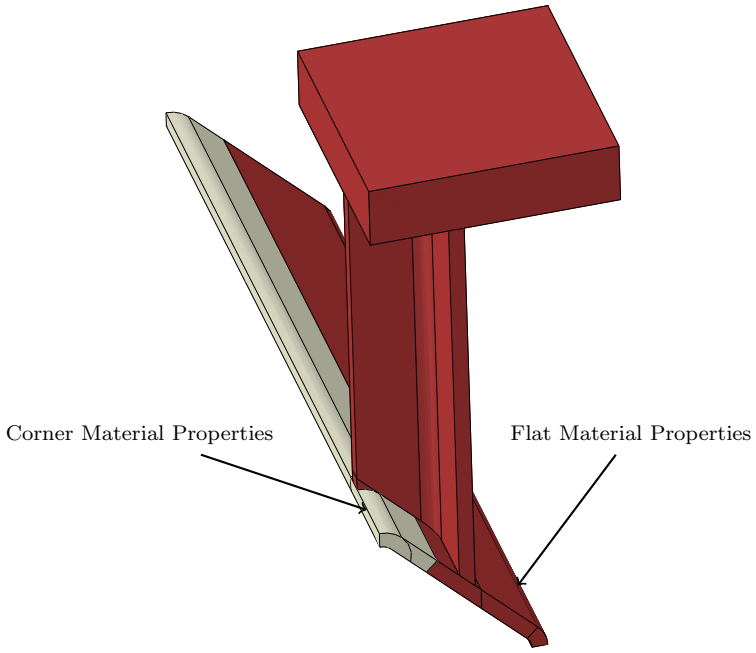

Figure 4.6: X-Specimen Material Assignments

4.3.3 IDEA StatiCa T-specimens

DOFEMs were created for the T-specimens in both IDEA Connection and IDEA StatiCa as seen in Figures 4.8 and 4.7. IDEA Member allowed the author to efficiently model all components of the connections including connection pins, gusset plates, support framing, and base plates. The IDEA Member model also included geometric non-linear effects.

IDEA Connection T-Specimen Model

IDEA Connection does not allow the modeling of multiple connections, so only the center branch-to-chord connection was explicitly modeled, and the global behavior of the chord was represented by the elastic super element connected to the center node. All settings used in this connection model were identical to those described in Section 4.3.1. The IDEA StatiCa connection of the T-specimen model set-up can be seen in Figure 4.7.

The connection model was constrained at the end of the branch and was loaded at the chord ends. The chord ends were loaded with concentrated moments and shears that created

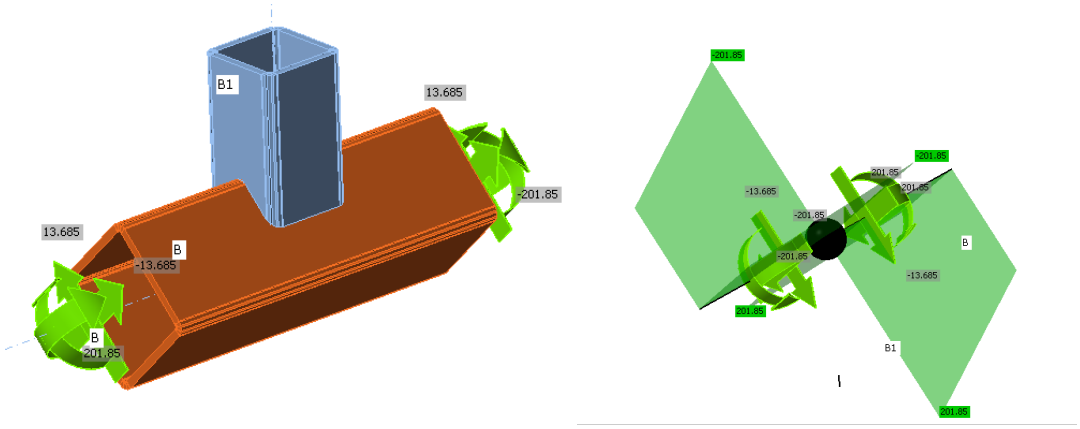

(a) (b)

Figure 4.7: (a) Idea Connection T-Model (b) IDEA Connection T-Model Internal Forces

the correct internal forces at the center of the joint. It can be seen in Figure 4.7 that the shears and moments at the cut chord end were not orthogonal to the branch force direction, instead, the shears and moments were placed at 45°from the vertical axis. This is because IDEA StatiCa requires forces and moments to be placed in line with the chord local axis. Since this chord was rotated, so were the forces. To account for this the loads were input in a way that would cause their effects to cancel out in the horizontal direction and combine in the vertical direction to create the correct effect at the branch location.

4.3.4 IDEA Member T-Specimen Model

The IDEA StatiCa Member model can be seen in Figure 4.8. In this connection all components of the test set-up were explicitly modeled; this model included all end plates, pins, and support columns that were present in the physical tests. The model was also loaded at the top branch, just as in the physical test.

4.3.5 Abaqus T-Specimens

The T-specimen was modeled as an assembly of multiple parts, as seen in Figure 4.10. The branch and chord of the T-section were modeled as one part. Similar to the X-specimen the joints were assumed to utilize a Complete Joint Penetration weld to join the branch and

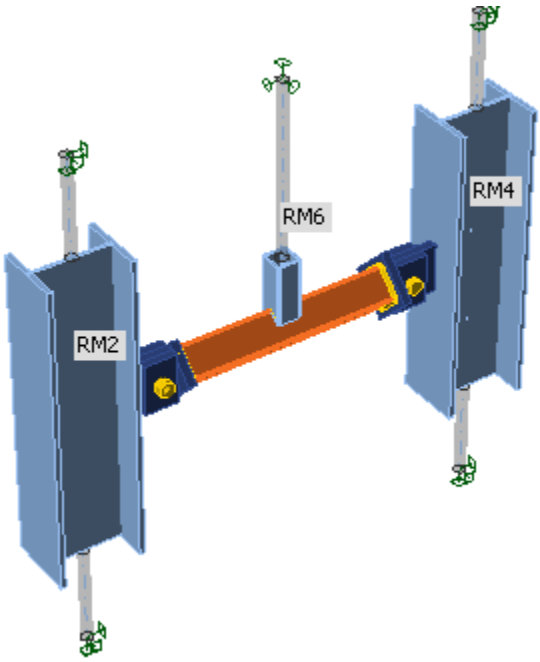

Figure 4.8: T-Specimen, Idea Member

chord and again, to represent this in the numerical model, two situations were considered. One T-model was created with a continuous mesh between the chord and nominal thickness branch and one model was created with a continuous mesh between the chord and branch, with the branch thickness including the thickness of the backer sleeve. The results from both models can be seen in Figure 4.3. These results suggest that the inclusion of the backer sleeve only minimally affects connection stiffness.

Also included in these models was a solid representation of the 1 $\frac{1}{2}$ inch connection pin, the support plates on the end of the chord, the support assembly with gussets and base plate, the load table, and the bolts connecting the base plate to the load table. Nominal dimensions were used for all parts, besides the pin and bolt holes. The pin and bolt holes were modeled to perfectly match the diameter of the associated fastener, to avoid instabilities before contact was initialized. Nominal dimensions on all parts were used instead of measured dimensions, to more accurately represent the workflow of a practicing engineer; typically, due to monetary and time constraints, all members cannot be measured before calculations are performed.

To simulate contact between all parts the powerful General Contact setting was used in Abaqus. The General Contact setting allows Abaqus to search for contact between all

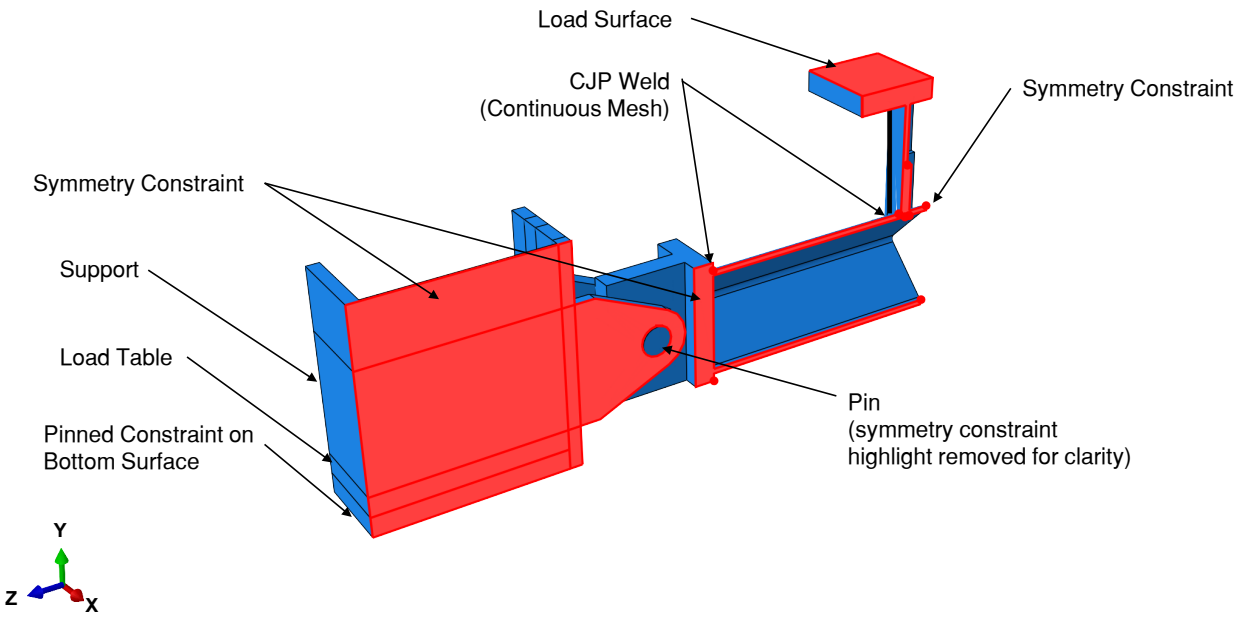

Figure 4.9: Abaqus Model Setup

surfaces in a model, including surfaces of the same solid. This thorough search allows the program to find contacts as the simulation evolves that the user may have otherwise missed. All default contact settings were used in the General Contact properties, besides in the tangent direction, where a penalty factor of 0.5 was used to account for friction between each steel component.

The body of the chord and branch of the T-section was meshed very similarly to the X-specimen. A global mesh size of 0.1 inches was assigned and a minimum number of elements through the thickness was set to 3, using the mesh size by curve option in Abaqus. 10-noded quadratic TET elements were used to mesh this solid. The geometry of all other components in the model were easily partitioned and allowed for use of more efficient HEX elements. A mesh size of 0.1 inches was used for the pin and gussets. A common mesh size constraint was used between the chord support plates, pin, and support gussets to ensure proper contact was made between all parts. The mesh size was kept consistent, because if it isn't, nodes may penetrate the neighboring surface causing over-closure issues, or may be outside of the contact search distance, causing instabilities.

The author placed constraints on the model as seen in Figure 4.9. To constrain this

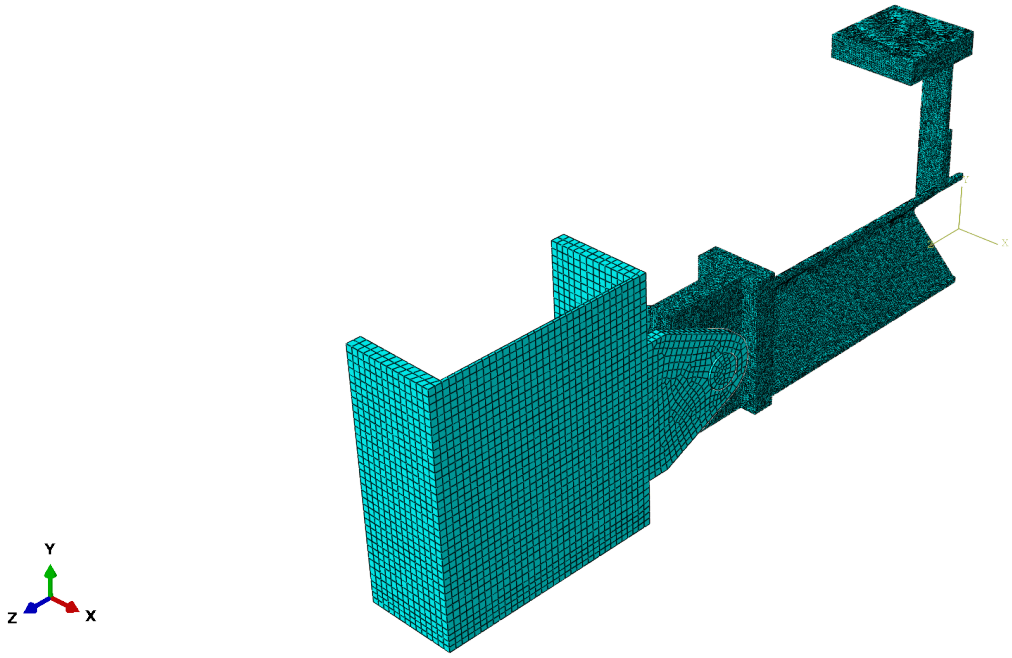

Figure 4.10: Abaqus Mesh

model a symmetry constraint was placed on the cut portions of the model and the bottom surface of the plate representing the load table was assigned pin constraints (u_x=u_y=u_z=0).

As discussed in Section 3.1.3 the process of forming an HSS strain hardens the corner of the section. To account for this the chords were partitioned in the Abaqus model to allow the stiffer corner material properties to be assigned as seen in 4.12. The corner material properties were extended $0.5 * \pi * r$ per the results of Chapter 3.

4.4 Results and Discussion

The results of all numerical models discussed in this Chapter are combined in Figures 4.15, 4.16, 4.18, and 4.17. Figures 4.15 and 4.16 show the results for the T-specimens, which were connected at their ends to pinned supports and allowed to bend at mid-span. Figures 4.18 and 4.17 show the results for the X-specimens, which were loaded via a top branch and supported by a bottom branch, with no eccentricity from the force location.

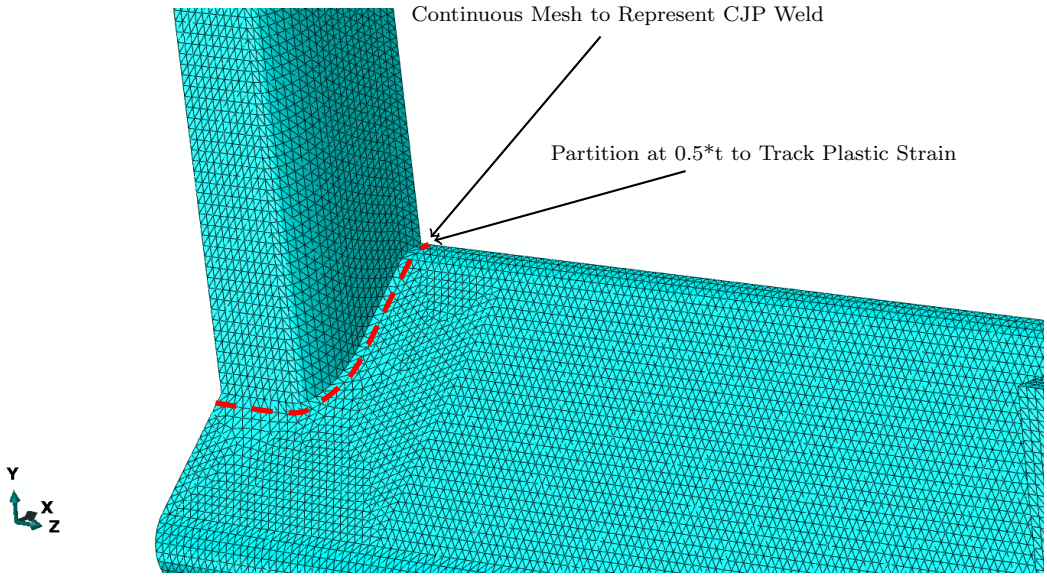

Figure 4.11: T-Specimen Branch-Chord Mesh

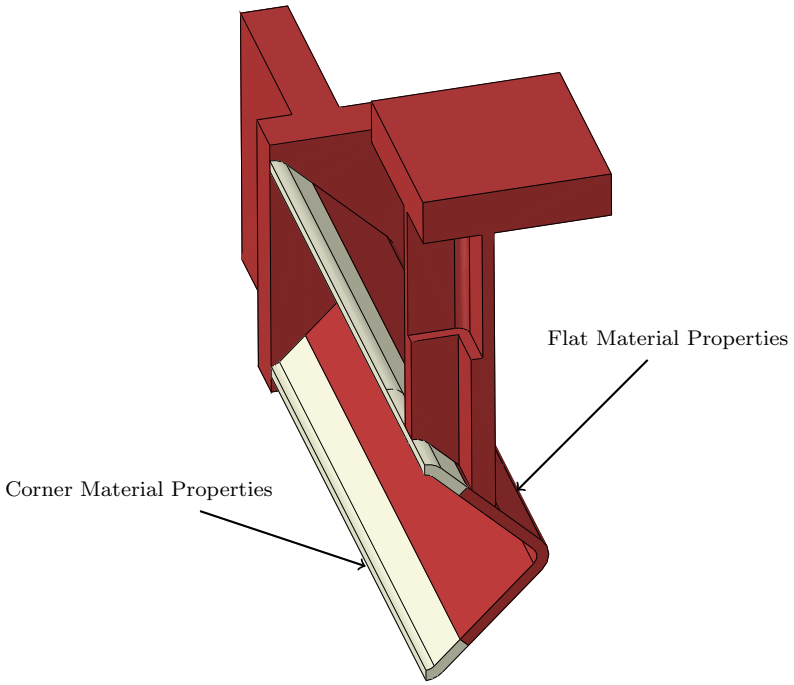

Figure 4.12: T-Specimen Material Assignments

4.4.1 Measuring Local Deflection

In each of the force-displacement graphs in this Section, the applied reaction force is plotted on the y-axis, and the local deformation of the chord face is plotted on the x-axis. Local displacement of the chord face is a deformation limit state that can be used to define the ultimate load of a connection when no obvious peak load is present on the load-deformation curve [44] [49]. The CIDECT Design Guide 3 for Tubular Structures and Eurocodes Part 1-14 both reference a 3% local deformation limit as an ultimate load criteria; however, they do not explicitly state what reference point should be used when measure the local deformation. CIDECT references a 1994 paper by Lu et al. [44] as the basis of the recommendation. A review of the 1994 paper shows that local deformation was measured by subtracting the bottom chord displacement from the branch displacement. It is reasonable to predict that the shape of a bird beak connection may significantly alter the local deformation results measured using this process.

Local deformation is automatically calculated in IDEA StatiCa, but in Abaqus, it must be determined by the user. It can be seen in Figures 4.15 and 4.16 that four methods were considered for calculating the local deformation from the Abaqus models. The first two methods required the user to measure the deflection of a node on the loading surface and a node on either the bottom corner of the HSS (similar to the Lu's seminal work) or the side corner; these reference nodes can be seen in Figure 4.13. The displacement of the bottom and side node were then subtracted from the displacement of the node on the loading surface to determine the local deformation as shown in Equations 4.1 and 4.2 and Figure 4.13. These results are labeled Abaqus (Center Node) and Abaqus (Bottom Node) in the Figures.

$$\delta_{local} = \delta_{loading} - \delta_{node1} \tag{4.1}$$

$$\delta_{local} = \delta_{loading} - \delta_{node2} \tag{4.2}$$

The third method required the user to calculate the theoretical deflection of the chord

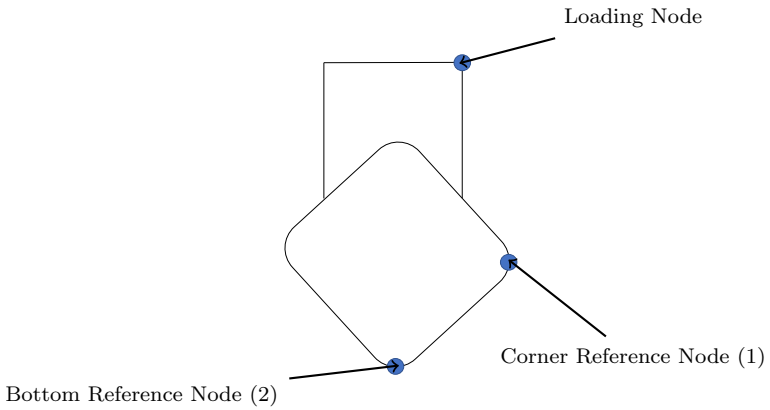

Figure 4.13: Local Deformation Reference Nodes

using elastic beam theory. The theoretical deflection was then subtracted from the displacement of a node on the top loading surface, as shown in Equation 4.4. This conversion process applies to the T-specimen models only, as the local and global displacements are identical for X-specimens.

$$\delta_{local} = \delta_{loading} - \frac{pl^3}{48EI} \tag{4.3}$$

The fourth method used to calculate local deformation was a combination of methods one and two. In this method, the author attempted to find the average deformation of the global cross-section by using an average displacement of the corner reference node (1) and bottom reference node (2). An example cross-section can be seen in Figure 4.14. In this example, the green line is the original cross-section, and the purple line is the deformed cross-section. It can be seen that the corner node and bottom node have different displacement values. By averaging these two values together, the global displacement of the cross-section may be approximated. The results seen in Figures 4.15 and 4.16 suggest that this method for calculating local deformation most closely agrees with the local deformations reported in IDEA StatiCa and is likely a reliable method for calculating serviceability limits for design; However, further research is likely needed to develop a more accurate weighted average method. An extensive experimental and numerical testing program should be carried out to determine the local deformation at peak loading of various bird beak connection geometries.

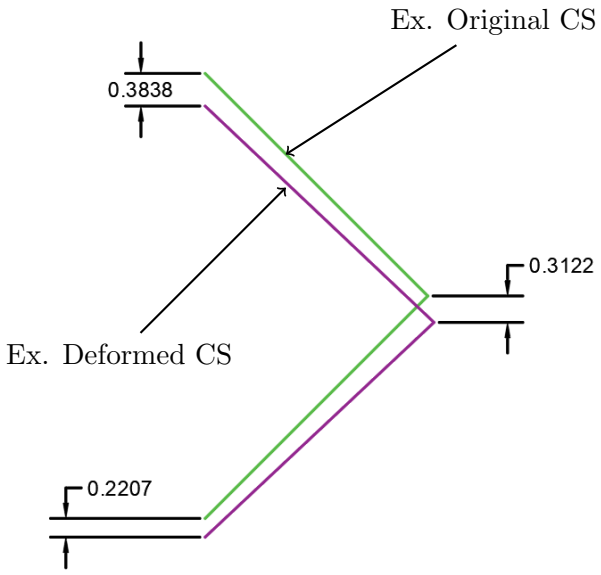

Figure 4.14: Local Deformation of Cross Section

$$\delta_{local} = \delta_{loading} - \frac{\delta_{node1} + \delta_{node2}}{2} \tag{4.4}$$

4.4.2 T-Specimen

The results of several model types and post-processing methods are shown in Figures 4.15 and 4.16. The model types considered are explained in Section 4.3. As explained in Section 4.4.1 the reported results of the Abaqus models are dependent on the method used to measure local deformation of the cross-section; all four methods explained in 4.4.1 are plotted in Figures 4.15 and 4.16.

Compression Results

It can be seen in Figure 4.15 that the Force-Displacement plot produced from the Abaqus model is significantly affected by the method used to convert global displacements to local deformations. When using the corner node as a reference node (Method 1), the Abaqus model appears to be stiffer than the IDEA StatiCa model in the linear and non-linear regions. However, when the bottom node is used as a reference (Method 2) or when elastic beam theory is used (Method 3) to measure a reference deflection, the Abaqus model appears

to be more flexible than the IDEA StatiCa model. When the average deformation of the bottom and corner node (Method 4) is used, the Abaqus model appears to be slightly more flexible than both IDEA StatiCa models in the linear region and significantly stiffer in the non-linear region. This result is expected and suggests that Method 4 is likely the most similar method to the one used in the IDEA StatiCa software.

The strength limits in Abaqus (5% plastic strain) are unchanged by the method used to convert global displacement to local deformation. The results show that the Abaqus model predicts a significantly higher strength than the IDEA StatiCa model and the AISC equations for planar connections. The Abaqus model predicts an ultimate connection capacity of 45.4 kips, the IDEA StatiCa model with nominal material properties (48 ksi yield) predicts an ultimate connection capacity of 32.52 kips and the IDEA StatiCa model with true material properties (58 ksi yield) predicts an ultimate connection capacity of 39.85 kips. The IDEA Member model predicts an ultimate connection capacity of 32.9 kips, and the AISC empirical equation for planar connections predicts an ultimate connection capacity of 41.34 kips.

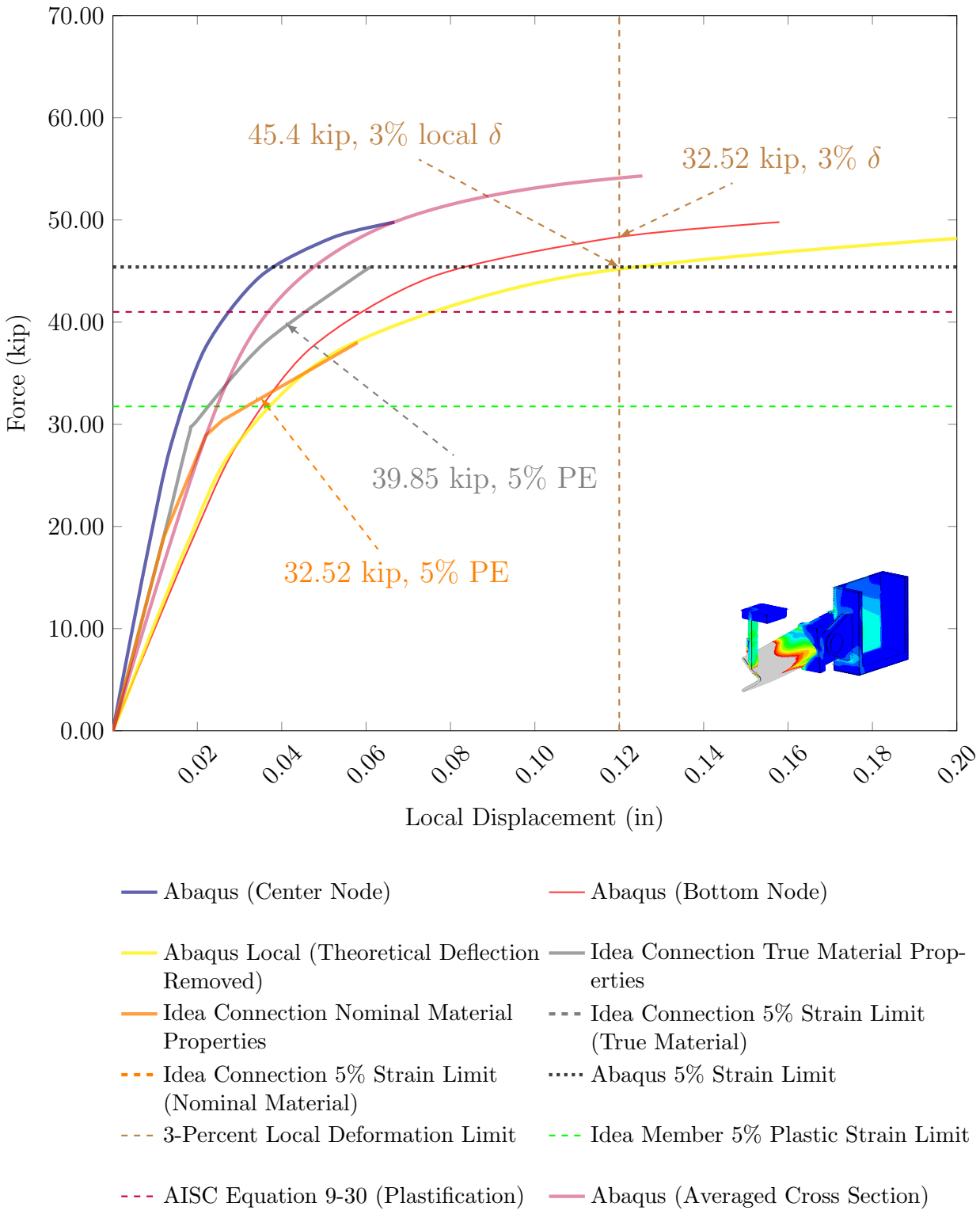

Figure 4.15: T-Specimen Compression Results

Tension Results

The results of the tension simulations are very similar to the compression results. It can be seen in Figure 4.16 that global to local deformation conversion Methods 2 and 3 tend to show that the Abaqus model is more flexible than the IDEA StatiCa models; Method 1 suggests that the Abaqus model is stiffer than the IDEA StatiCa models. Method 4 shows that the Abaqus model is slightly more flexible than the IDEA StatiCa models in the linear region and significantly stiffer in the non-linear region. The strength limits are also similar to the compression results. The Abaqus model predicted an ultimate connection capacity of 50.1 kips, the IDEA StatiCa model with nominal material properties predicted a capacity of 35.8 kips, the IDEA StatiCa model with true material properties predicted a capacity of 44.64 kips, and the AISC empirical equation predicted a connection capacity of 41.34 kips.

Summary

The ultimate capacity limits shown in Figures 4.15 and 4.16 are as expected. The Abaqus models are expected to predict a much higher capacity than the IDEA StatiCa models because the Abaqus models include complete stress-strain material models with strain hardening. The IDEA StatiCa models, on the other hand, are modeled with elastic-plastic material with a nominal yielding slope. These results suggest that the Abaqus ROFEM model has predicted an accurate connection capacity, and all versions of IDEA StatiCa have predicted conservative connection capacities.

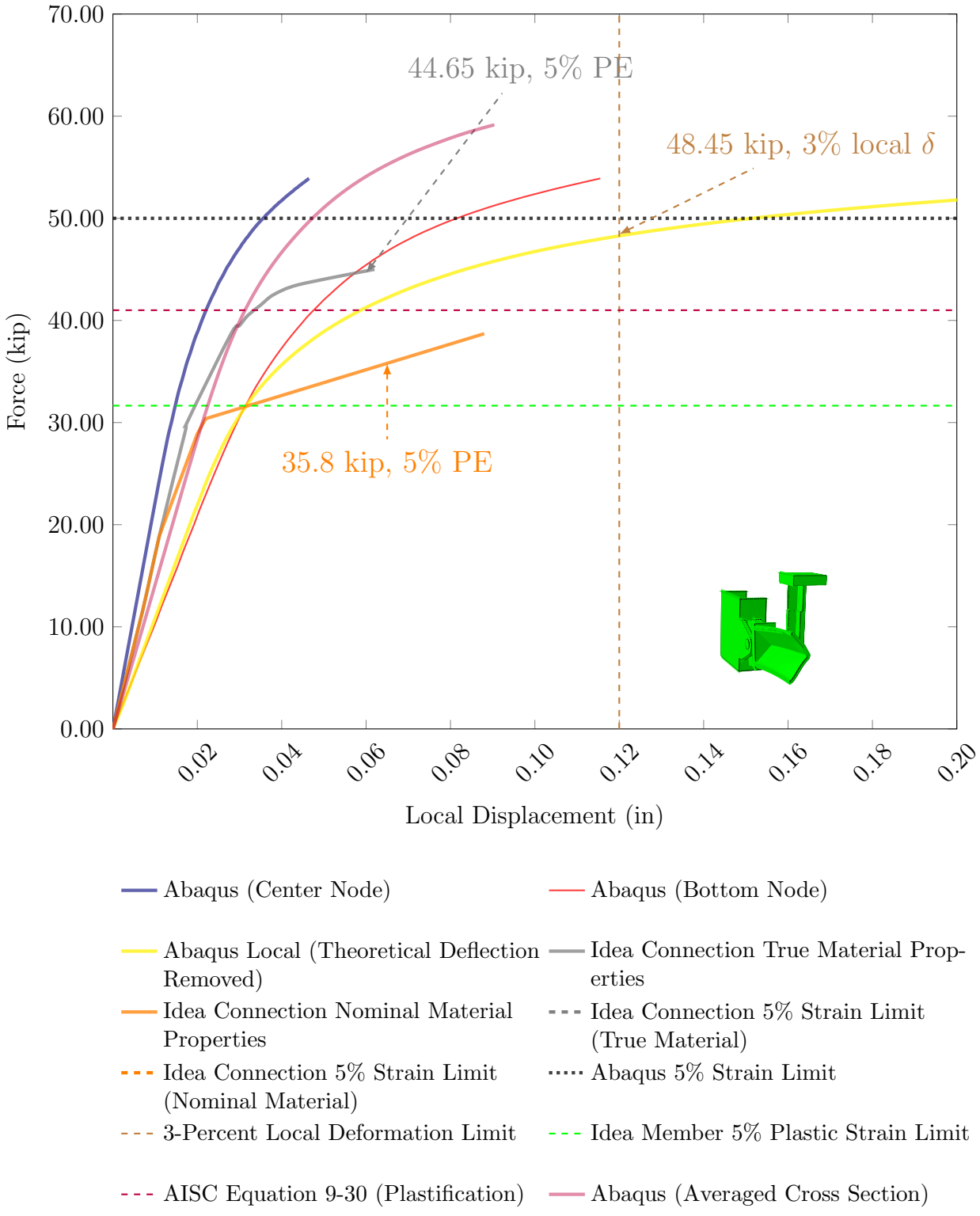

Figure 4.16: T-Specimen Tension Results

4.4.3 X-Specimen

As described in Sections 4.3.1 and 4.3.2, three total numerical models were created to predict the capacity of the X-specimens. Unlike the T-Specimen, the X-Specimen configuration was not allowed to bend globally and was also modeled with 1/8th symmetry, which means there was no bottom node to use as a reference plane. The middle node (node 1 in Figure 4.13) sat directly on a plane of symmetry; therefore, by definition, it could not displace in the vertical axis. For these reasons, multiple methods of converting global displacement to local deformation were not necessary.

Compression Results

As can be seen in Figure 4.18, the reduced complexity of measuring local deformations appears to create more consistent results than those shown in Section 4.4.2. Figure 4.18 shows that the Abaqus model and IDEA StatiCa models made with nominal and true yield material models have almost identical stiffness in the linear region, and then results diverge after yielding. After yielding the IDEA StatiCa model with a nominal material model (48 ksi yield) is significantly more flexible than the other models. The IDEA StatiCa model made with a true material model (58 ksi yield) maintains its stiffness for longer due to its elevated yield capacity but quickly "relaxes" at about 0.06 inches of local displacement and the stress-strain curve flattens out. The Abaqus model, made with a complete non-linear material model, remains far stiffer than the IDEA StatiCa models in the non-linear range.

It can be seen in Figure 4.18 that the IDEA StatiCa models predict the lowest connection capacity. The IDEA StatiCa Nominal Material model predicts an ultimate connection capacity of 28.1 kips. The IDEA StatiCa True Material model predicts an ultimate capacity of 33 kips. Lastly, the Abaqus model predicted a capacity of 49.8 kip. These model results can be compared to a capacity predicted by the AISC empirical equation of 41.34 kip. Just as explained in Section 4.4.2 these results are exactly as expected, due mainly to the difference in material properties used in each model. The capacity of the Abaqus model to strain harden allows it to maintain stiffness and limit the increase in plastic strain far better than the IDEA StatiCa models, which conservatively use elastic-plastic material models. The

inherent conservatism of IDEA StatiCa makes it ideal for use as a design tool; in this case the results may even be excessively conservative and lead to an excessively robust connection design.

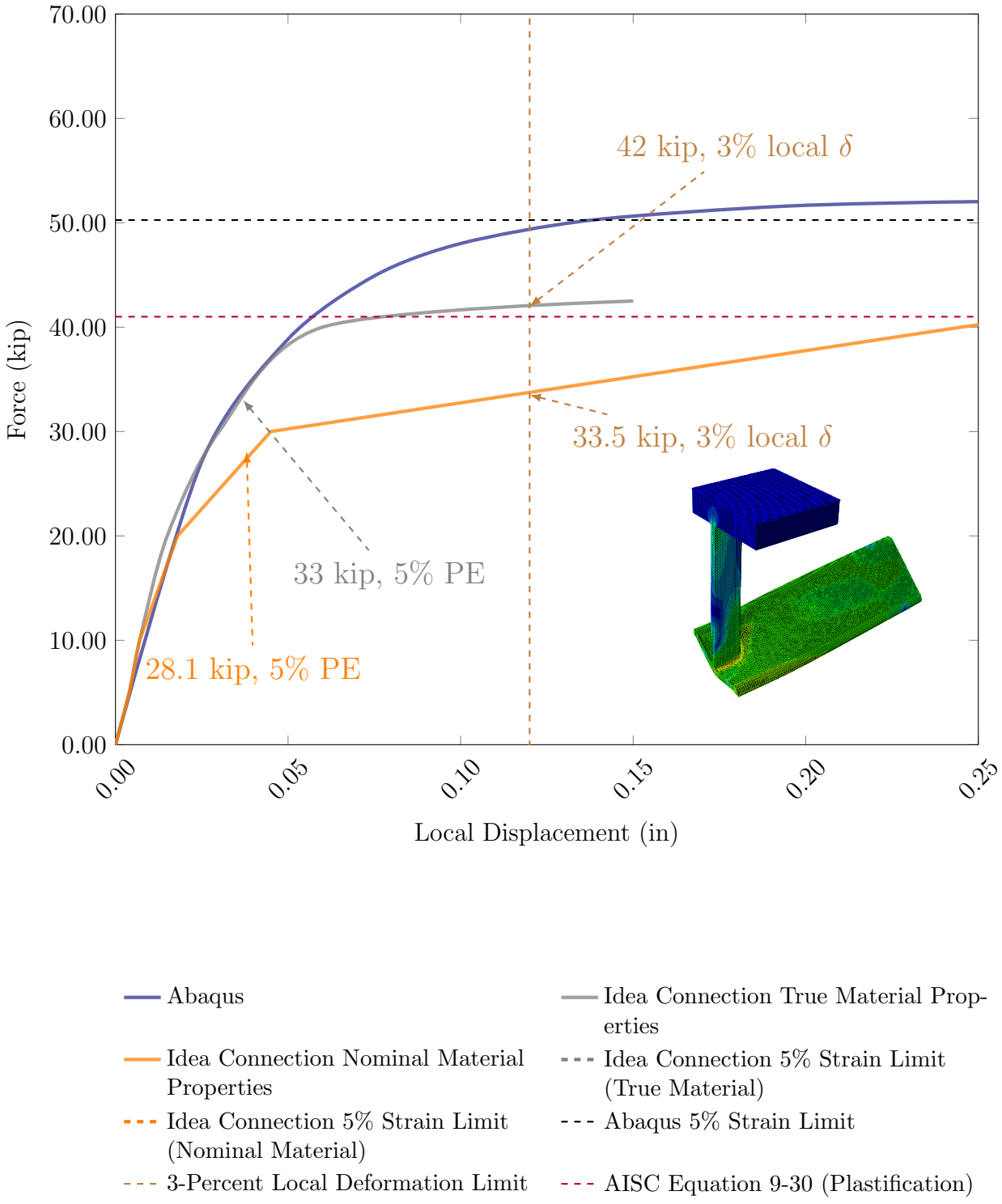

Figure 4.17: X-Specimen Compression Results

Tension Results

As was the case for the T-Specimen, the relative flexibility of the X-Specimen models in tension is similar to the compression results. All three models have almost identical stiffness in the linear region. In the non-linear region, the IDEA StatiCa Nominal model is the most flexible, followed by the IDEA StatiCa True Material model and the Abaqus model.

The trend in the connection capacities is also the same in the tension results compared to the compression results; however, the difference between the Abaqus capacity and IDEA StatiCa results is even larger. In the tension case, the Abaqus model predicted a connection capacity of 58.2 kips, while the IDEA Connection Nominal and True Material Property models predicted a capacity of 28.5 kips and 35 kips, respectively. These results can be compared to the AISC empirical design value of 41.34 kip. This again demonstrates that IDEA StatiCa is a safe design tool, that produces conservative results, but also suggests that a design completed with IDEA StatiCa may produce an overly robust connection, compared to a design completed with a detailed ROFEM.

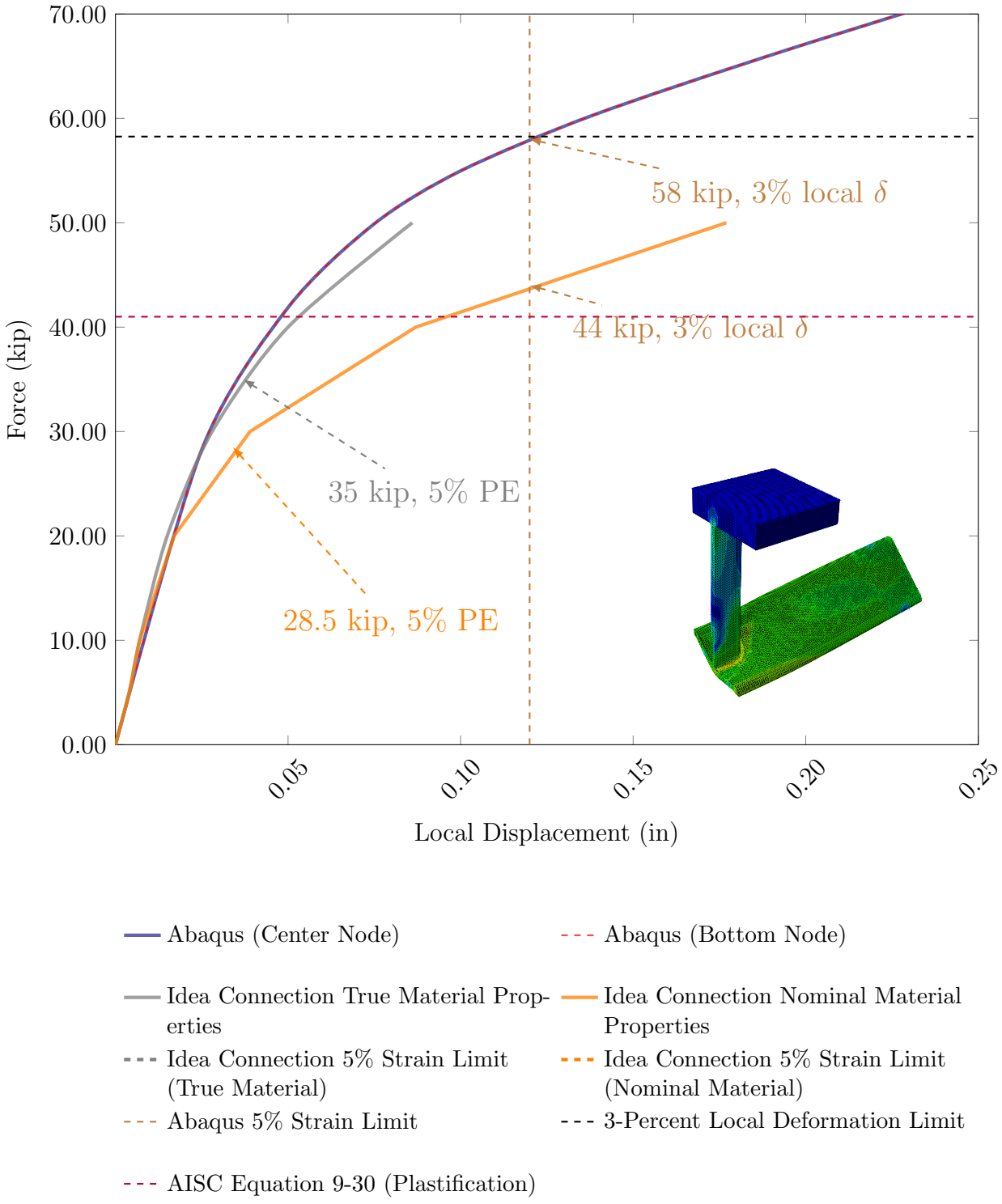

Figure 4.18: X-Specimen Tension Results

Summary

The consistent trend in the data for the X-Specimen was that IDEA StatiCa and Abaqus predicted similar stiffness results in the linear region and Abaqus predicted a stiffer connection in the non-linear region. Abaqus also predicted a far stronger connection in both tension and compression cases. As explained in this section it appears that a connection designed with IDEA StatiCa would be conservative and designed with significant excess capacity. A connection designed with Abaqus would likely lead to a more economical design, which would provide the level of safety intended in the controlling design code. However, this is not to be considered a limitation of IDEA StatiCa. The purpose of IDEA StatiCa is to be a design tool for practicing engineers. The feature that allows Abaqus to be more accurate, and less conservative, is the complete non-linear material diagram that is included in the model. It is extremely rare that a design engineering firm would perform material testing to create material diagrams for a commercial design; this would be cost and time prohibitive. This is why IDEA StatiCa uses an elastic-plastic material model, which facilitates the design of connections with code-provided yield values only.

AISC Nominal Ultimate Strength:

As stated in Section 2.5 there are two primary modes of failure considered in this thesis (1) punching shear and (2) chord wall plastification. The AISC Steel Construction Manual provides two methods for checking punching shear in HSS connections. In Commentary K1.1 of the 15th edition manual, the use of inelastic finite element analysis is explicitly allowed for connections that do not meet the limitations shown in Chapter K. This chapter gives a limiting inelastic, or plastic, strain value of 0.02/T where T is the thickness of the chord wall, for the connections shown herein this limit is 8%. Punching shear can also be checked with Equation 9-29 of the manual, which gives the shear rupture strength of a flat plate based on the connection's effective width as described in Section K1.2. The effective width equation has been derived from research on transverse plate to HSS connections [23]. The punching shear equation provided in the AISC manual is calculated by multiplying the Von Mises shear yielding stress ($0.6F_y$) by the effective area of the connection. This effective area equation was derived for flat plates connected to the face of Rectangular HSS Sections and

does not account for the increased stiffness at the center of a bird beak connection. Stress states in HSS connections are non-uniform and are higher at high stiffness regions of the chord, typically at the chord walls. In bird beak connections, the stiffness of the connection is highest at the centerline of the member, where the branch connects to the chord corner. There are currently no known code formulae for punching shear in bird beak connections, nor non-planar connections. See equation 4.5 for the nominal ultimate punching shear strength for the analagous planar connection to compare to the bird beak connections studied in this chapter. For this connection the punching shear strength does not control.

AISC Punching Shear Equation 9-29:

$$R_n := 0.6 \cdot F_y \cdot t \cdot (2 \cdot c_{eff} + 2 \cdot L) = 65.55\text{kip} \tag{4.5}$$

Where:

F_y = Yield Stress of Chord

t = Thickness of Chord Wall

b_1 = Width of Branch

b_0 = Width of Chord

c_{eff} = Effective Width of Branch, per Equation 4.6

L = Branch Depth

$$c_{eff} = (\frac{10t}{2B}) + (\frac{f_y * t}{F_{yb} t_b}) B_b = 1.73in \tag{4.6}$$

The second failure mode considered in this thesis, chord wall plastification, occurs due bending of the chord face and is dominant in flexible connections. This failure mode can be

checked per the AISC manual equation 9-30 for out-of-plane transverse loads. This equation represents a yield line approach. This approach involves using the virtual work method to determine the external work that must be performed to exceed the internal energy caused by rotation of the chord face at the yield lines at failure. This process has been simplified by AISC using Equation 4.7 below.

Chord Transverse Plastification Equation 9-30:

$$R_n : \frac{t^2 \cdot F_y}{2} \cdot \left[\frac{(a+b) \cdot \left(4 \cdot \sqrt{\frac{T \cdot a \cdot b}{a+b}} + L\right)}{a \cdot b} \right] = 41.358 \text{ kip} \tag{4.7}$$

F_y = Yield Stress of Chord

t = Thickness of Chord Wall

B_b = Width of Branch

B = Width of Chord

a = Distance from Left Side to Edge of Branch

b = Distance from Right Side to Edge of Branch

T = Unbraced Length of HSS Chord Face

Punching Forces in FEA Models

Additional Abaqus models were created to better understand the distribution of shear forces in the studied bird beak connection, as well as "standard" planar HSS connections. The author created two shell models representing the experimental X-specimen and Planar X-connection with the same shapes, dimensions, and material properties. The author then applied a forced displacement of 0.4 inches in the tension direction to the top of the branches; this displacement was meant to represent the 3% local deformation limit of the connection. Figures 4.23 and Figure 4.21 show the internal shear force distribution of the two models. It can be seen in the figures that the shear force distribution in the planar connection matches well with the theoretical distribution anticipated, as shown in Figure 4.19. The stiffness in

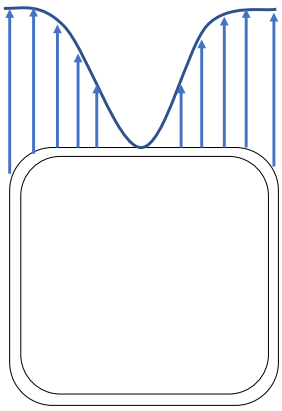

Figure 4.19: Assumed Punching Shear Distribution

the connection is concentrated at the chord walls, and thus the majority of the internal force in the chord is also concentrated at the walls; very little shear force is distributed to the center of the chord. The distribution in the bird beak connection is similar; however, the bird beak connection has relatively high stiffness in the "middle" of the connection at the corner of the chord, which allows the chord to better distribute the shear forces to the chord corner in the middle of the connection and into the chord face near the edge of the connection. This distribution of forces results in a lower peak shear stress in the chord material at the local deformation limit.

When looking at the force distribution diagram, it is clear why the effective width c_{eff} is used to reduce the punching shear capacity of HSS chords. As stated previously, the force in HSS connections is attracted towards the stiffer portion of the chord, typically the sidewalls, as shown in Figure 4.19. The effective width equation does not suggest that an area smaller than the branch will fail in rupture; Rather, a small area on the weld perimeter will be subjected to highly concentrated forces. Only a fraction of the weld perimeter will be required to support/distribute the internal forces. In contrast, the rest of the perimeter remains essentially unloaded; this phenomenon can be seen in Figure 4.21.

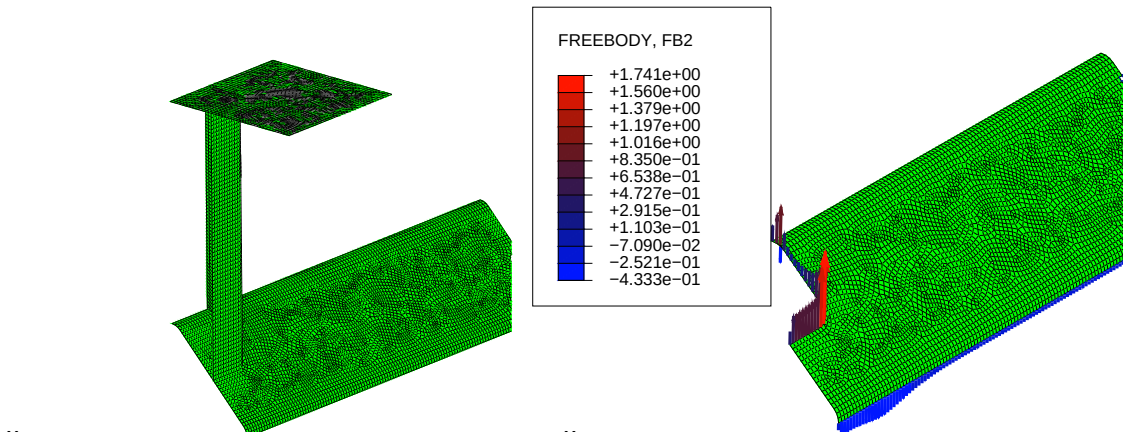

Figure 4.20: Shear Distribution Bird Beak Connection

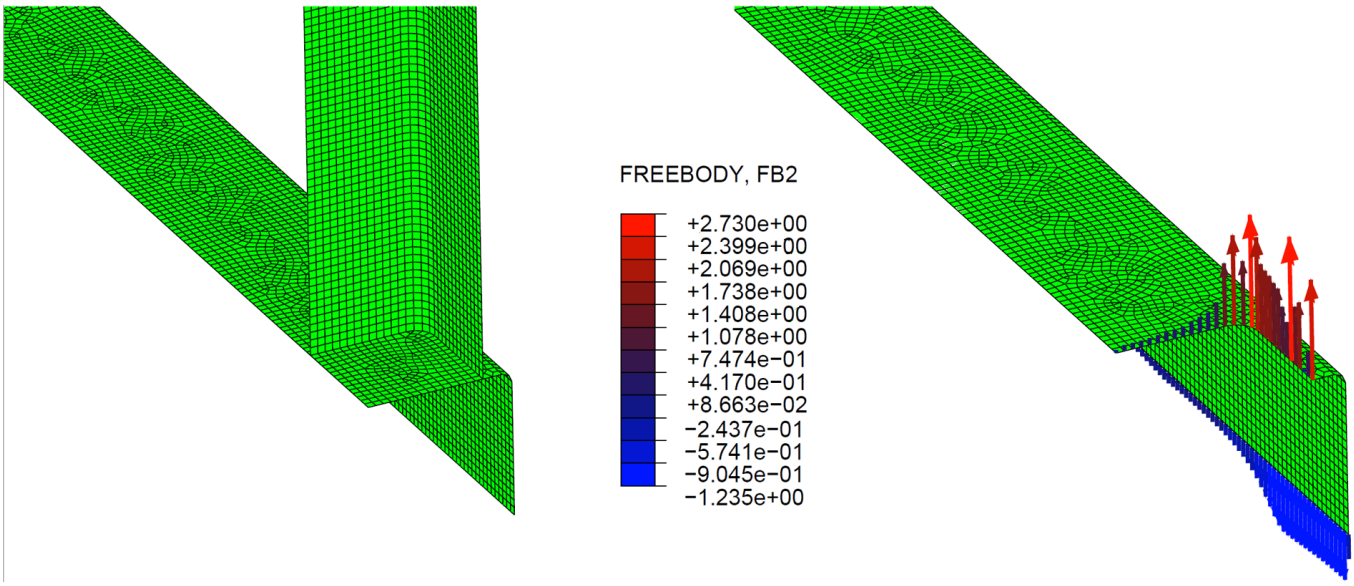

Figure 4.21: Shear Distribution Planar Connection

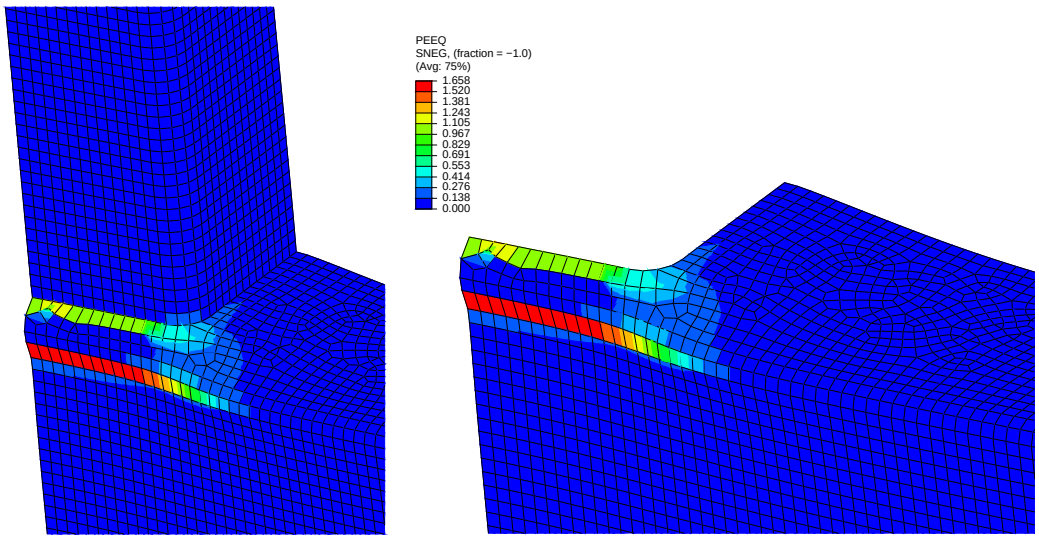

Figure 4.22: Shear Distribution Bird Beak Connection

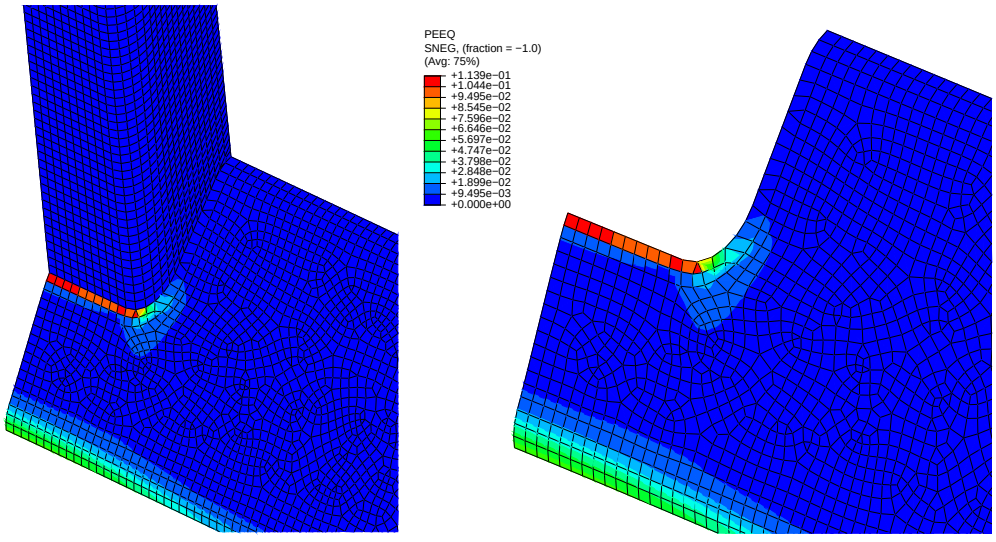

Figure 4.23: Shear Distribution Bird Beak Connection

Chapter 5

Conclusions and Recommendations

The current prevailing design codes in North America and Europe (AISC 360, CIDECT, and Eurocodes) do not provide design provisions for non-planar RHS joints with branches placed at arbitrary angles. These connections are sometimes preferred for roller coasters, oil platforms, architectural features, and other special structures. Since no known empirical design equations are available for these connections a general analysis type is needed. A general analysis method often used is the Finite Element Method (FEM). The FEM is a powerful tool that is used often in the Aerospace, Naval, and Civil industries to analyze complex structural-mechanical assemblies. This research evaluated the ability of General Purpose Finite Element software (Abaqus) and Component Based Finite Element software (IDEA StatiCa) to accurately predict the strength and deformation characteristics of non-planar RHS joints.

In this research widely used, and previously verified, finite element programs were used to determine the capacity of RHS joints. First, experimental results of planar RHS joints were used to validate numerical modeling methods as seen in Chapter 3. These validated modeling methods were then used to create an expanded numerical study as seen in Chapter 4.1, which determined the strength of bird beak RHS connections using a ROFEM, a DOFEM, and empirical equations for an analagous planar connection. As already stated, there are no code formulae available for non-planar connections. There is also no code formulae available for

square bird beak connections, such as the one studied in Chapter 4.1. The nearest empirical equations available for comparison to this data are those for traditional planar HSS as found in Chapter K of the AISC manual.

When comparing the numerical results in the ROFEMs to the available planar empirical equations it can be seen that the ROFEM created in Abaqus predicts a significantly higher connection capacity. This is likely due to the increased stiffness of the connection caused by connecting directly to the strain hardened corner of the chord. The analogous planar connection to the bird beak connection studied in Chapter 4.1 is controlled by chord wall plastification and has significant excess punching shear capacity. The increased stiffness of the bird beak connection significantly increased the chord wall plastification strength and thus, in this case, the connection strength. This phenomena is likely to exist in non-planar connections, which means utilizing general purpose FEA for design of these connections could allow designers to take advantage of significantly more strength. The design oriented finite element program (IDEA Statica) however, did not demonstrate increased connection capacity and actually agreed well with the empirical equations for the planar analogue connection. As stated in this thesis IDEA Statica does not take into account the strain hardening of the chord corners or non-linear material properties of the chord.

The research program referenced in this thesis was too limited to definitively answer the research question; however, the results of this research do give a strong indication that both General Purpose and Component Based FEM are capable of predicting the strength and deformation characteristics of non-planar joints made with RHS members. The FEM models created in Abaqus proved capable of predicting the relevant System Response Quantities (SRQs) within 5% of the experimental test results in all comparisons (where experimental data was available) and showed a significant improvement in capacity for bird beak connections compared to the equivalent planar analogue. The FEM models created in IDEA StatiCa included nominal material properties and member dimensions and consistently provided conservative results when compared to experimental data.

5.1 Further Studies

To fully validate the finite element design approach proposed in this paper further experimental research is needed. This study was limited by the testing equipment commonly available in university laboratories, which do not allow for testing of true non-planar connections. The author of this paper believes that the experimental geometries considered capture the relevant phenomenology of non-planar connections; however, it is conceivable that, when a true non-planar connection is tested, unique failure phenomena may occur that has not been identified in this paper. A more extensive experimental program is needed, which includes connections with multiple non-planar branches, loaded with varying directional forces (tension, compression, and moment) to verify the results of this study.

This study is also limited to connections with uniaxial compression/tension forces only. In reality, these non-planar joints will often be loaded with moment and torsional forces as well as axial forces. The author of this paper believes it is prudent to perform additional testing on non-planar connections with applied moment and axial forces before using the recommendations in this paper in practical design. The author believes it is acceptable to use IDEA StatiCa for these applications without further testing, thanks to their extensive verification and validation efforts on many connection types.

The bird beak connections studied in Chapter 4.1 were compared to planar connections that were controlled by chord wall plastification and thus a significant increase in strength was shown in the stiffer bird beak variation of the connection. However, it is not as immediately clear that a bird beak configuration will improve the punching shear capacity of the connection as the increase in stiffness in the connection may increase stress concentrations and localize the large inelastic strains over a smaller area. The author recommends that this study is extended with connections in the punching shear critical zone with $0.85 < \beta < \frac{1}{\gamma} or \frac{B}{t} < 10$.

The author also recommends more research on other methods to create non-planar RHSS connections, such as cast connections. Cast connections may allow design engineers to specify non-planar RHS connections without the need for finite element analysis, or special weld provisions. Cast connections move all welds up the branch of a member, away from

the complex geometry of the connection "node". The use of cast connections also transfers the node design to the cast connection company, which may be better suited to perform advanced finite element analyses, due to the specialty nature of the company and the ability to develop a library of experimental results for validation and verification.

Bibliography

[1] Examining spatial (grid) convergence. URL https://www.grc.nasa.gov/www/wind/valid/tutorial/spatconv.html.

[2] Miguel Abambres and Mario Rui Arruda. Finite element analysis of steel structures–a review of useful guidelines. *International Journal of Structural Integrity*, 2016.

[3] Nabil Abdel-Rahman and KS Sivakumaran. Material properties models for analysis of cold-formed steel members. *Journal of Structural Engineering*, 123(9):1135–1143, 1997.

[4] AISC. *Steel construction manual*. American institute of steel construction, 2017.

[5] ANSYS FLUENT ANSYS. version 14.0: user manual. ansys. *Inc., Canonsburg, USA*, 2011.

[6] Jørgen Apeland. Application of fe-analysis in design and verification of bolted joints according to vdi 2230 at cern. Master's thesis, NTNU, 2018.

[7] P Arasaratnam, KS Sivakumaran, and MJ Tait. True stress-true strain models for structural steel elements. *International Scholarly Research Notices*, 2011, 2011.

[8] I Assessment and II Assessment. Connection design by component based finite element method.

[9] Brad L Boyce, Sharlotte LB Kramer, H Eliot Fang, Theresa E Cordova, Michael K Neilsen, K Dion, Amy K Kaczmarowski, Erin Karasz, Liang Xue, Andrew J Gross, et al. The sandia fracture challenge: blind round robin predictions of ductile tearing. *International Journal of Fracture*, 186(1-2):5–68, 2014.

[10] Xiao-Ding Bu and Jeffrey A Packer. Chord end distance effect on rhs connections. *Journal of Constructional Steel Research*, 168:105992, 2020.

[11] William D Callister Jr and David G Rethwisch. *Callister's materials science and engineering*. John Wiley & Sons, 2020.

[12] G. Cantin and Clough RW. A curved cylindrical shell finite element. volume 6, 01 1968. doi: 10.2514/6.1968-176.

[13] G. Cantin and Clough RW. A curved cylindrical shell finite element. volume 6, 01 1968. doi: 10.2514/6.1968-176.

[14] YS Choo, GJ Van der Vegte, N Zettlemoyer, BH Li, and JYR Liew. Static strength of t-joints reinforced with doubler or collar plates. i: Experimental investigations. *Journal of Structural Engineering*, 131(1):119–128, 2005.

[15] AO Cifuentes and A Kalbag. A performance study of tetrahedral and hexahedral elements in 3-d finite element structural analysis. *Finite Elements in Analysis and Design*, 12(3-4):313–318, 1992.

[16] Ray Clough and Edward Wilson. Dynamic finite element analysis of arbitrary thin shells. *Computers Structures - COMPUT STRUCT*, 1:33–56, 08 1971. doi: 10.1016/0045-7949(71)90004-6.

[17] Ray Clough and Richard Woodward. Analysis of embankment stresses and deformations. *Journal of Soil Mechanics and Foundation Division*, 93:529–549, 07 1967. doi: 10.1061/JSFEAQ.0001005.

[18] Ray W Clough. The finite element method after twenty-five years: a personal view. *Computers & Structures*, 12(4):361–370, 1980.

[19] Ray W Clough and Edward L Wilson. *Stress analysis of a gravity dam by the finite element method*. Laboratório Nacional de Engenharia Civil, 1962.

[20] Structural Welding Code-Steel. Aws d1. 1/d1. 1m. *American Welding Society*, 2010.

[21] MG Coutie and G Davies. The behaviour of three dimensional rectangular hollow section tee joints under axial branch loads. In *Tubular Structures V*, pages 444–451. CRC Press, 2004.

[22] G Davies and P Crockett. The strength of welded t-dt joints in rectangular and circular hollow section under variable axial loads. *Journal of Constructional Steel Research*, 37 (1):1–31, 1996.

[23] Gwynne Davies and Jeffrey A Packer. Predicting the strength of branch plate–rhs connections for punching shear. *Canadian Journal of Civil Engineering*, 9(3):458–467, 1982.

[24] Hyeong Do Kweon, Jin Weon Kim, Ohseop Song, and Dongho Oh. Determination of true stress-strain curve of type 304 and 316 stainless steels using a typical tensile test and finite element analysis. *Nuclear Engineering and Technology*, 53(2):647–656, 2021.

[25] Dan Dubina, Raffaele Landolfo, and Viorel Ungureanu. Design of cold-formed steel structures.: Eurocodes part 1-14: Design assisted by finite element analysis gives guidance for material non-linear analysis. Eccs, 2021.

[26] Ehab Ellobody, Ran Feng, and Ben Young. *Finite element analysis and design of metal structures*. Elsevier, 2013.

[27] YuJing Fan. *RHS-to-RHS axially loaded X-connections offset towards an open chord end*. PhD thesis, University of Toronto (Canada), 2017.

[28] Pazmino Marcos Bryan Flores. The prediction of the joint stifness of riveted steel bridges. Master's thesis, České vysoké učení technické v Praze. Vypočetní a informační centrum., 2018.

[29] Oscar Minor García. *The Impact of the Connection Stiffness on the Behaviour of a Historical Steel Railway Bridge*. PhD thesis, Master Thesis, Prague, 2017.

[30] https://www.ideastatica.com/support-center/tekla-structures-bim-link-for-connection design. Tekla structures tutorial for connection - bim link. 2022.

[31] Thomas JR Hughes. *The finite element method: linear static and dynamic finite element analysis*. Courier Corporation, 2012.

[32] JP Jaspart and K Weynand. Design of hollow section joints using the component method. *Tubular Structures XV*, pages 403–410, 2015.

[33] Kenneth Kavanagh and Ray Clough. Finite element application in the characterization of elastic solid. *International Journal of Solids and Structures - INT J SOLIDS STRUCT*, 7:11–23, 01 1971. doi: 10.1016/0020-7683(71)90015-1.

[34] Martin Kožich, Petr Jehlička, FrantiŠek Wald, Xiao-Ding Bu, Jeffrey A Packer, and JAROMÍR Kabeláč. Towards establishing a design resistance for hollow section joints. In *Proc., 17th Int. Symp. on Tubular Structures*, pages 643–650, 2019.

[35] Jens Kuhn, Jeffrey A Packer, and YuJing Fan. Rectangular hollow section webs under transverse compression. *Canadian Journal of Civil Engineering*, 46(9):810–827, 2019.

[36] L Kwaśniewski. Application of grid convergence index in fe computation. *Bulletin of the Polish Academy of Sciences: Technical Sciences*, (1), 2013.

[37] Hyeong Do Kweon, Eun Ju Heo, Do Hwan Lee, and Jin Weon Kim. A methodology for determining the true stress-strain curve of sa-508 low alloy steel from a tensile test with finite element analysis. *Journal of Mechanical Science and Technology*, 32(7):3137–3143, 2018.

[38] Yun Ling. Uniaxial true stress-strain after necking. *AMP Journal of technology*, 5(1): 37–48, 1996.

[39] DK Liu and J Wardenier. 40 static strength of multiplanar dx-joints in rectangular hollow sections. 1993.

[40] DK Liu and J Wardenier. Multiplanar influence on the strength of shs multiplanar kk-joints. In *international conference on tubular structures*, pages 203–212. Swets and Zeitlinger, 2001.

[41] DK Liu and J Wardenier. The strength of multiplanar gap kk-joints of rectangular hollow sections under axial loading. In *The Eleventh International Offshore and Polar Engineering Conference*. OnePetro, 2001.

[42] DK Liu and J Wardenier. The strength of multiplanar overlap kk-joints of rectangular hollow sections under axial loading. In *The Twelfth International Offshore and Polar Engineering Conference*. OnePetro, 2002.

[43] DK Liu and J Wardenier. The strength of multiplanar kk-joints of square hollow sections. In *Tubular Structures X*, pages 197–205. Routledge, 2017.

[44] LH d Lu, GD De Winkel, Y Yu, and J Wardenier. Deformation limit for the ultimate strength of hollow section joints. In *Tubular structures VI*, pages 341–347. Routledge, 2021.

[45] G Martinez-Saucedo, JA Packer, and S Willibald. Parametric finite element study of slotted end connections to circular hollow sections. *Engineering structures*, 28(14): 1956–1971, 2006.

[46] Peter Matic. Numerically predicting ductile material behavior from tensile specimen response. *Theoretical and applied fracture mechanics*, 4(1):13–28, 1985.

[47] Hossein Moravej, Shojaeddin Jamali, Tommy Chan, and Andy Nguyen. Finite element model updating of civil engineering infrastructures: A literature review. In *Proceedings of the 8th International Conference on Structural Health Monitoring of Intelligent Infrastructure 2017*, pages 1–12. International Society for Structural Health Monitoring of Intelligent ..., 2017.

[48] Jeffrey A Packer. Fe-based design of hss connections.

[49] Jeffrey A Packer, Jaap Wardenier, Xiao-Ling Zhao, GJ Van der Vegte, and Yoshiaki Kurobane. *Design guide for rectangular hollow section (RHS) joints under predominantly static loading*. Cidect, 2009.

[50] Jeffrey A Packer, Donald Sherman, and Maura Lecce. *Hollow structural section connections*. American Institute of Steel Construction Chicago, IL, 2010.

[51] Stuart Pawsey and Ray Clough. Improved numerical integration of thick shell finite elements. *International Journal for Numerical Methods in Engineering*, 3:575 – 586, 10 1971. doi: 10.1002/nme.1620030411.

[52] RS Puthli and PUTHLI RS. Geometrical non-linearity in collapse analysis of thick shells, with application to tubular steel joints. 1981.

[53] Patrick J Roache. *Verification and validation in computational science and engineering*, volume 895. Hermosa Albuquerque, NM, 1998.

[54] L Šabatka, F Wald, J Kabeláč, L Gödrich, and J Navrátil. Component based finite element model of structural connections. In *Proceedings of the 12th International Conference on Steel, Space & Composite Structures*, volume 28, page 30, 2014.

[55] Teseo Schneider, Yixin Hu, Xifeng Gao, Jeremie Dumas, Denis Zorin, and Daniele Panozzo. A large scale comparison of tetrahedral and hexahedral elements for finite element analysis. *arXiv preprint arXiv:1903.09332*, 2019.

[56] Leonard E Schwer. Is your mesh refined enough? estimating discretization error using gci. *7th LS-DYNA Anwenderforum*, 1(1):45–54, 2008.

[57] Michael Smith. Abaqus/standard user's manual, version 6.9. 2009.

[58] Min Sun. *Mechanical Behaviour of Cold-Formed Hollow Structural Section Material*. University of Toronto (Canada), 2014.

[59] Kyle Tousignant and Jeffrey A Packer. Numerical investigation of fillet welds in hss-to-rigid end-plate connections. *Journal of Structural Engineering*, 143(12):04017165, 2017.

[60] M Jon Turner, Ray W Clough, Harold C Martin, and LJ Topp. Stiffness and deflection analysis of complex structures. *journal of the Aeronautical Sciences*, 23(9):805–823, 1956.

[61] GJ Van der Vegte, CHM De Koning, RS Puthli, and J Wardenier. Numerical simulation of experiments on multiplanar tubular steel x-joints. *International Journal of Offshore and Polar Engineering*, 1(03), 1991.

[62] GJ van der Vegte, Jaap Wardenier, and Ram S Puthli. Fe analysis for welded hollow-section joints and bolted joints. *Proceedings of the Institution of Civil Engineers-Structures and Buildings*, 163(6):427–437, 2010.

[63] Andrew P Voth and Jeffrey A Packer. Numerical study and design of t-type branch plate-to-circular hollow section connections. *Engineering Structures*, 41:477–489, 2012.

[64] František Wald, Jaromír Kabeláč, Marta Kuříková, Ondřej Perháč, Pavel Ryjáček, Oscar Minor, Marcos Bryan Flores Pazmiño, Lubomír Šabatka, and Drahoslav Kolaja. Advanced procedures for design of bolted connections. In *IOP Conference Series: Materials Science and Engineering*, volume 419, page 012044. IOP Publishing, 2018.

[65] František Wald, L Šabatka, Miroslav Bajer, P Jehlička, J Kabeláč, M Kožich, Marta Kuříková, and M Vild. *Component-based finite element design of steel connections*. Czech Technical University, 2020.

[66] K Weynand, E Busse, and J-P Jaspart. First practical implementation of the component method for joints in tubular construction. In *Tubular Structures XI*, pages 139–145. Routledge, 2017.

[67] S Willibald, JA Packer, and RS Puthli. Bolted connections for rhs tension members. *CIDECT Project D*, 8, 2001.

[68] Xiao-Ling Zhao. Deformation limit and ultimate strength of welded t-joints in cold-formed rhs sections. *Journal of constructional steel research*, 53(2):149–165, 2000.

Appendix A

Fabrication Drawings

REVISIONS				
REV	ZONE	DESCRIPTION	DATE	APPROVED
A			AUTHORITY	APPROVED:
			REL DATE	DRAFTER:

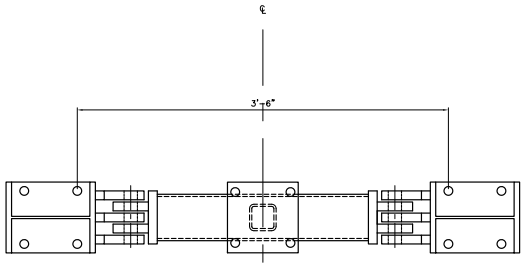

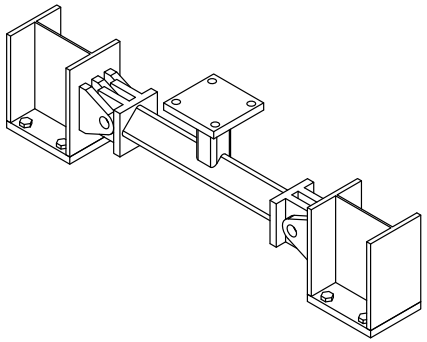

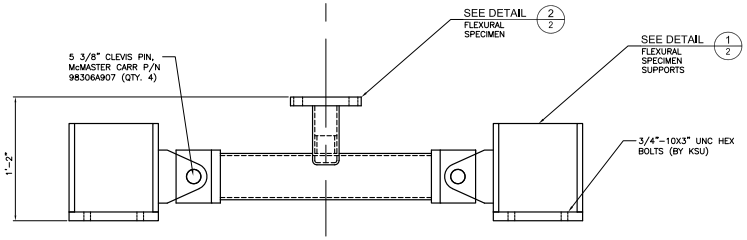

FLEXURAL TEST SPECIMEN ASSEMBLY
SCALE: 1:8

GENERAL NOTES

1. HARDWARE TO BE PURCHASED BY KSU

KANSAS STATE UNIVERSITY

DRAWN BY	AL KNOX	7/29/21
ENGINEER	AL KNOX	7/29/21
TIP TIMER		
PROJECT		
CHECKER	DR. JONES	
RELEASE DATE		
DRAWING NO.		

KSU RESEARCH PROJECT
FLEXURAL TEST SPECIMEN
DETAIL SHEET

SIZE	CAGE CODE	DRAWING NO.	REV
E		KSU-1001	A
SCALE	NOTED	ABC	SHEET 1 OF 2

REVISIONS				
REV	ZONE	DESCRIPTION	DATE	APPROVED
A			AUTHORITY	APPROVED
			REL DATE	DRAFTER

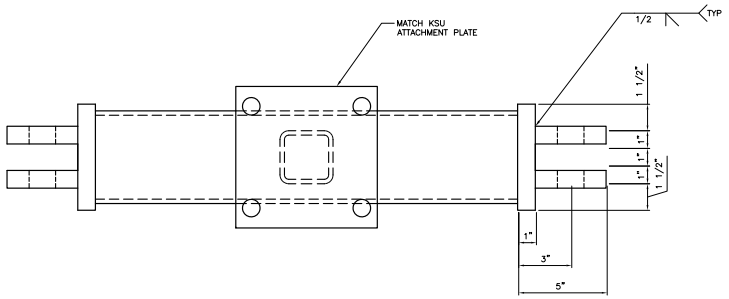

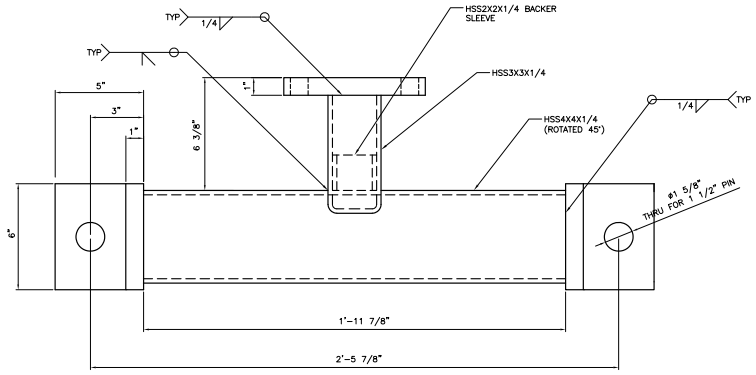

SEE DETAIL 2
FLEXURAL
SPECIMEN
QTY: 3

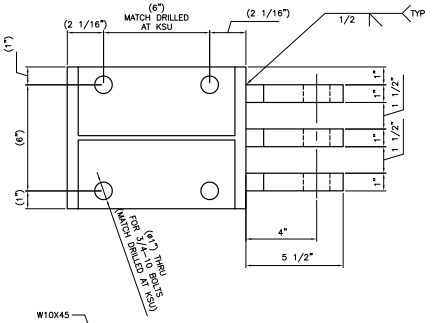

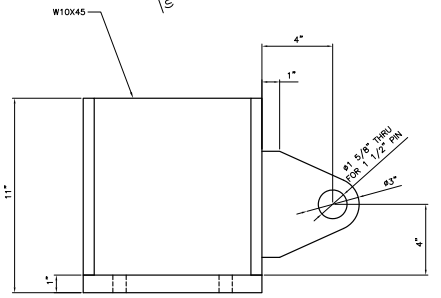

SEE DETAIL 1
FLEXURAL
SPECIMEN
SUPPORTS
QTY: 2

GENERAL NOTES

1. ALL PLATE TO BE A572 GR.50 STEEL UNLESS OTHERWISE NOTED
2. ALL HSS TO BE A500 GR.C UNLESS OTHERWISE NOTED
3. WELD ELECTRODES TO BE E70XX UNLESS OTHERWISE NOTED
4. ALL DIMENSIONS IN PARANTHESES ARE REFERENCE ONLY
5. WORK MARKED "AT KSU" WILL BE COMPLETED BY KSU'S TECHNICIANS, ALL OTHER WORK TO BE COMPLETED BY PKM STEEL
6. ALL COMPONENTS AT CENTERLINE UNLESS OTHERWISE NOTED

KANSAS STATE UNIVERSITY

DRAWN BY	N. KNOX	7/29/21
ENGINEER	N. KNOX	7/29/21
SUPERVISOR		
PROJECT		
CHECKER	DR. JONES	
RELEASE DATE		
DRAWING NO.		

KSU RESEARCH PROJECT
FLEXURAL TEST SPECIMEN
DETAIL SHEET

SIZE	CAGE CODE	DRAWING NO.	REV
E		KSU-1001	A
SCALE	NOTED	SHEET	2 OF 2

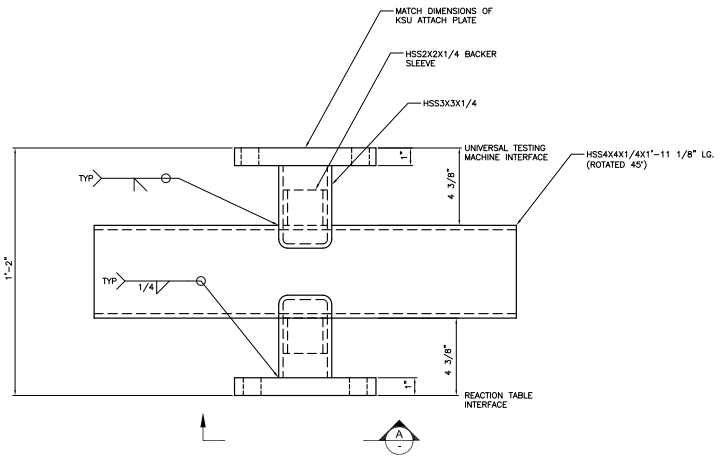

T-CONNECTION TEST SPECIMEN ASSEMBLY
SCALE: 1:2
QTY: 3

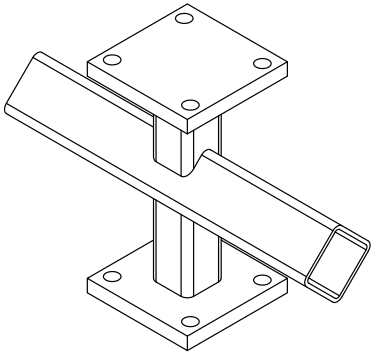

T-CONNECTION TEST SPECIMEN ISOMETRIC VIEW
SCALE: 1:2

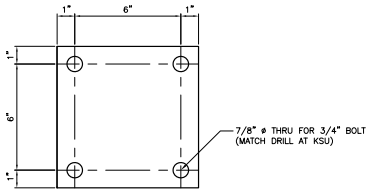

SECTION A
SCALE: 1:2

GENERAL NOTES

1. ALL PLATE TO BE A572 GR.50 STEEL UNLESS OTHERWISE NOTED
2. ALL HSS TO BE A500 GR.C UNLESS OTHERWISE NOTED
3. WELD ELECTRODES TO BE E70XX UNLESS OTHERWISE NOTED
4. ALL DIMENSIONS IN PARANTHESES ARE REFERENCE ONLY
5. ALL COMPONENTS AT CENTERLINE UNLESS OTHERWISE NOTED

REVISIONS				
REV	ZONE	DESCRIPTION	DATE	APPROVED
A			AUTHORITY:	APPROVED:
			REL DATE:	DRAFTER:

KANSAS STATE UNIVERSITY

DRAWN BY	N. KINCH	7/29/21	
ENGINEER	N. KINCH	7/29/21	
QP ENGR			
PROJECT			
CHECKER	DR. JONES		
RELEASE DATE		B	
DSWG NO.		1	

KSU RESEARCH PROJECT
T-CONNECTION SPECIMEN ASSEMBLY & DETAILS

SIZE	CAGE CODE	DRAWING NO.	REV
E		KSU-1002	A
SCALE	NOTED	ABC	SHEET 1 OF 1